Non-canonical activation of IRE1α during *Candida albicans* infection enhances macrophage fungicidal activity

Michael J. McFadden [1], Mack B. Reynolds [1], Britton C Michmerhuizen [1,a], Einar B. Ólafsson [1], Faith M. Anderson [1], Tracey L. Schultz [1], Mary X.D. O'Riordan[†] [1], Teresa R. O'Meara[†] [1]

Affiliations:

[1] Department of Microbiology and Immunology, University of Michigan, Ann Arbor, MI 48109, USA.

Michael J. McFadden; mcfaddmj@umich.edu, Mack B. Reynolds; mbreyn@umich.edu, Britton C Michmerhuizen; michmer8@msu.edu, Einar B. Ólafsson; olaffson@umich.edu, Faith M. Anderson; faithma@umich.edu, Tracey L. Schultz; tracschu@umich.edu, Teresa R. O'Meara; tromeara@umich.edu, Mary X.D. O'Riordan; oriordan@umich.edu

[a] Current affiliation: College of Human Medicine, Michigan State University, Grand Rapids, MI 49503, USA.

[†] Corresponding author

Correspondence to tromeara@umich.edu or oriordan@umich.edu

Abstract

While the canonical function of IRE1α is to detect misfolded proteins and activate the unfolded protein response (UPR) to maintain cellular homeostasis, microbial pathogens can also activate IRE1α, which modulates innate immunity and infection outcomes. However, how infection activates IRE1α and its associated inflammatory functions have not been fully elucidated. Recognition of microbe-associated molecular patterns can activate IRE1α, but it is unclear whether this depends on protein misfolding. Here, we report that a common and deadly fungal pathogen, *Candida albicans,* activates macrophage IRE1α through C-type lectin receptor signaling, reinforcing a role for IRE1α as a central regulator of host responses to infection by a broad range of pathogens. This activation did not depend on protein misfolding in response to *C. albicans* infection. Moreover, lipopolysaccharide treatment was also able to activate IRE1α prior to protein misfolding, suggesting that pathogen-mediated activation of IRE1α occurs through non-canonical mechanisms. During *C. albicans* infection, we observed that IRE1α activity promotes phagolysosomal fusion that supports the fungicidal activity of macrophages. Consequently, macrophages lacking IRE1α activity displayed inefficient phagosome maturation, enabling *C. albicans* to lyse the phagosome, evade fungal killing, and drive aberrant inflammatory cytokine production. Mechanistically, we show that IRE1α activity supports phagosomal calcium flux after phagocytosis of *C. albicans*, which is crucial for phagosome maturation. Importantly, deletion of IRE1α activity decreased the fungicidal activity of phagocytes *in vivo* during systemic *C. albicans* infection. Together, these data provide mechanistic insight for the non-canonical activation of IRE1α during infection, and reveal central roles for IRE1α in macrophage antifungal responses.

Introduction

Intracellular infection by diverse pathogens triggers cell stress programs, such as the unfolded protein response (UPR), whose three branches (IRE1α, PERK, and ATF6) have broad consequences for host antimicrobial defenses through regulation of innate immunity, cellular metabolism and homeostasis, and cell differentiation or cell death pathways[1–4]. Canonically, accumulation of misfolded proteins in the ER lumen triggers activation of the UPR[5]. As proteostasis is required for cellular function, UPR activation can restore cellular homeostasis by modulating gene expression to promote protein folding and expansion of the ER network. Alternatively, failure to overcome proteotoxic stress leads to cell death[5]. Therefore, initiation of the UPR during infection may be critical to circumvent the effects of pathogen virulence factors, support the production of secreted proteins such as cytokines through cooperation with proinflammatory transcription factors, or to regulate organelle contact sites for inter-organelle

60 communication[4,6,7]. Still, the utility and effects of UPR activation during infection are not fully
61 understood and differ in response to individual pathogens, which may differentially exploit UPR
62 activation for pathogenesis[8–15].

63 After detecting misfolded protein accumulation in the ER lumen, IRE1α assembles into
64 small oligomers that allow its *trans*-autophosphorylation[16]. Autophosphorylation of IRE1α results
65 in activation of its endonuclease domain, allowing IRE1α to remove a short intronic sequence
66 from the *Xbp1* transcript in a non-canonical mRNA splicing reaction, orthologous to the Ire1-*Hac1*
67 splicing reaction that drives the UPR in yeast[17–19]. *Xbp1* splicing results in a frameshift within the
68 open reading frame, allowing translation and protein synthesis of the transcription factor XBP1S,
69 which promotes the transcription of genes involved in ER quality control[20]. However, the IRE1α
70 branch of the UPR can also be selectively triggered by infection or detection of microbe-
71 associated molecular patterns (MAMPs) by pattern recognition receptors (PRRs), such as Toll-
72 like receptors (TLRs)[6,21]. Additionally, the regulatory roles of IRE1α extend beyond XBP1S, as
73 IRE1α itself can modulate JNK pathway activation, orchestrate organelle contact sites, and
74 regulate metabolic plasticity[23,26,27,74]. Previous reports suggested that protein misfolding-
75 independent activation of IRE1α may occur following TLR stimulation, although this model has
76 not been directly tested[6,21].

77 IRE1α has broad regulatory roles and consequences for infection and immunity. For
78 example, the IRE1α-XBP1S axis can promote the expression of proinflammatory cytokines[6,22],
79 modulate metabolic plasticity[24], and promote ER homeostasis[25] during infection. Additionally,
80 IRE1α can facilitate intra-organelle communication for ER-mitochondria calcium signaling and
81 promotion of reactive oxygen species (ROS) generation[12,13,26]. Through its regulatory effects on
82 gene expression, metabolism, and redox balance, IRE1α can promote bacterial killing or
83 inflammasome activation in phagocytic cells[10,12]. Despite these known roles of IRE1α in bacterial
84 and viral infection, mechanistic understanding of IRE1α activation during infection is lacking.
85 Further, our understanding of the role of IRE1α during fungal infection is only beginning to
86 emerge.

87 Given its many functions in host responses to infection, we sought to understand the role
88 of IRE1α in macrophage interactions with *Candida albicans*. *C. albicans* is a common fungal
89 member of the human mucosal microbiota and an opportunistic pathogen[28]. Phagocytic cells are
90 an important early line of defense against systemic infection by *C. albicans*[29]. Macrophages and
91 neutrophils can recognize and phagocytose *C. albicans* predominantly through C-type lectin
92 receptor (CLR) signaling and eliminate infection through fungicidal activity or secretion of
93 cytokines to orchestrate antifungal immunity[30–33]. Interestingly, a recent report found that IRE1α

can be activated in neutrophils upon *C. albicans* infection, and IRE1α activity contributes to the immunopathology of systemic *C. albicans* infection[14], revealing the importance of regulation of this pathway during infection. However, the role of IRE1α in macrophage responses to *C. albicans* have not been investigated. Macrophages are crucial for early antifungal responses *in vivo* and are thought to control *C. albicans* dissemination through phagocytosis, direct antifungal activity, and cytokine signaling to recruit neutrophils to sites of infection[29,34,35]. During intracellular growth in macrophages, *C. albicans* hyphal formation can allow it to escape the phagosome and kill macrophages through lysis or programmed cell death through pyroptosis[36–41]. However, the mechanisms by which macrophages contain and kill *C. albicans* are incompletely understood. Indeed, levels of microbicidal effectors, such as ROS, are not reliable predictors of phagocyte fungicidal activity[42,43]. Recent work reported that lysosome fusion with the expanding *C. albicans*-containing phagosome is crucial to maintain phagosome integrity, prevent phagosomal rupture, and allow fungicidal activity[43–46]. Together, these findings suggests that phagosome maturation is a critical component of antifungal responses by macrophages.

Here, we report that IRE1α is activated in macrophages following infection by *C. albicans*. Importantly, IRE1α activation was dependent on CLR signaling, but did not depend on detectable accumulation of misfolded proteins, suggesting a non-canonical mechanism of activation. Additionally, we found IRE1α is dispensable for phagocytosis of *C. albicans* by macrophages, but contributes to their fungicidal activity *in vitro* and *in vivo*. Macrophages lacking IRE1α activity failed to efficiently recruit lysosomes to the phagosome, which was followed by increased phagosome rupture and more hyphal growth by *C. albicans*. These results reveal a role for IRE1α in the fungicidal capacity of macrophages, advancing our understanding of the emerging role of IRE1α in antifungal immunity.

Results

C. albicans infection results in activation of macrophage IRE1α

While the ER stress sensor IRE1α is activated in response to bacterial and viral infection, its role and activation in response to fungal infections is only beginning to emerge. To determine whether macrophage IRE1α is activated during *C. albicans* infection, we measured splicing of *Xbp1* mRNA in immortalized bone marrow-derived macrophages (iBMDM) infected with *C. albicans*, or treated with known IRE1α activating stimuli, bacterial lipopolysaccharide (LPS) or thapsigargin, as positive controls. Using semi-quantitative RT-PCR analysis of *Xbp1* mRNA, we observed that *C. albicans* infection induces *Xbp1* splicing in wild-type iBMDM (WT), albeit to a lesser extent than the positive controls LPS and thapsigargin (Fig. 1A). *Xbp1* splicing did not occur

128 in response to any of the treatments in a clonal iBMDM cell line lacking exons 20 and 21 of IRE1α
129 (IRE1$^{\Delta R}$), which are required for its endonuclease activity[47] (Fig. 1A, 1B). Analysis of *Xbp1* splicing
130 by RT-qPCR following a timecourse of *C. albicans* infection showed induction of *Xbp1-S* at 4
131 hours post-infection (hpi) with *C. albicans* (Fig. 1C). As the SC5314 reference strain can be an
132 outlier in virulence and hyphal formation[28,48], we measured *Xbp1-S* induction following infection
133 with a selection of commensal *C. albicans* isolates previously isolated from healthy donors[28] and
134 demonstrated that all isolates resulted in comparable *Xbp1* splicing to the reference strain
135 SC5314 (Fig. 1D).
136 *Xbp1* splicing leads to translation of the transcription factor XBP1S to induce the
137 transcription of ER quality control responsive genes following unfolded protein stress. However,
138 while LPS and thapsigargin treatment led to accumulation of XBP1S by 4 hpi, infection with *C.*
139 *albicans* did not lead to induction of XBP1S protein expression at 4, 6, or 8 hours post-infection
140 (Fig. S1). Thus, IRE1α function during *C. albicans* infection of macrophages is likely independent
141 of the transcription factor XBP1S. Together, these results indicate that *C. albicans* infection results
142 in mild activation of IRE1α in macrophages.
143
144 **C-type lectin receptor signaling drives TRAF6-independent IRE1α activation during *C.***
145 ***albicans* infection.**
146 C-type lectin receptors, which detect components of the cell wall of *C. albicans*[31], are the
147 major pattern recognition receptor for recognition of *C. albicans* in macrophages[49]. To determine
148 whether C-type lectin receptor (CLR) signaling contributes to IRE1α activation during *C. albicans*
149 infection, we measured *Xbp1* splicing in iBMDM lacking the CLR signaling adaptor protein CARD9
150 (CARD9 KO), compared to WT iBMDM. CARD9 was required for *Xbp1* splicing in response to *C.*
151 *albicans*, but dispensable for *Xbp1* splicing in response to LPS, which activates a distinct signaling
152 pathway through Toll-like receptor 4 (TLR4)[50,51] (Fig. 1E). These results suggest CLR signaling is
153 required for IRE1α activation in response to *C. albicans*. Next, we addressed whether CLR
154 agonism is sufficient to stimulate IRE1α activity by treating WT or IRE1$^{\Delta R}$ iBMDM with a Dectin-1
155 specific agonist, depleted Zymosan (d-Zymosan). We found that depleted Zymosan treatment
156 was sufficient to trigger IRE1α-dependent *Xbp1* splicing, demonstrating that CLR agonism
157 triggers IRE1α activity (Fig. 1F). Similar to results with *C. albicans* infection, *Xbp1* processing by
158 IRE1α was more strongly stimulated by LPS than by depleted Zymosan (Fig. 1F). Despite CLRs
159 being the major pattern recognition receptors for *C. albicans,* TLRs can also respond to fungal
160 cells[52]. To test whether TLR engagement is necessary for IRE1α activation in response to *C.*
161 *albicans*, we measured *Xbp1* splicing in BMDM lacking TLR2, TLR4, and TLR9 (TLR2/4/9 KO).

162 We observed a similar level of *Xbp1* splicing to WT iBMDM in response to *C. albicans* and
163 depleted Zymosan, although *Xbp1* splicing was ablated in response to LPS, as expected (Fig.
164 1G). Together, these results suggest CLR signaling is necessary and sufficient for IRE1α
165 activation in response to *C. albicans*.
166 TRAF6 is a crucial E3 ubiquitin ligase involved in innate immune signaling for both TLR
167 and CLR pathways[53,54]. This ubiquitin ligase can directly ubiquitinate IRE1α and facilitates the
168 ubiquitination and activation of IRE1α after LPS treatment[6,21]. Therefore, we tested whether
169 TRAF6 is involved in IRE1α activation in response to *C. albicans* infection. While knockout of
170 TRAF6 resulted in the expected decrease in *Xbp1* splicing in response to LPS, we observed that
171 *Xbp1* splicing in response to *C. albicans* infection was not affected by TRAF6 deletion (Fig. 1H).
172 Therefore, CLR-mediated IRE1α activation is TRAF6-independent. These data reveal that CLR
173 signaling through the adaptor protein CARD9 triggers IRE1α activation independently of TLR
174 signaling or TRAF6, in contrast to LPS-driven IRE1α activation, which depends on TLR signaling
175 to TRAF6. These data reveal a distinct mechanism of IRE1α activation in macrophages through
176 CLR signaling during fungal infection.
177

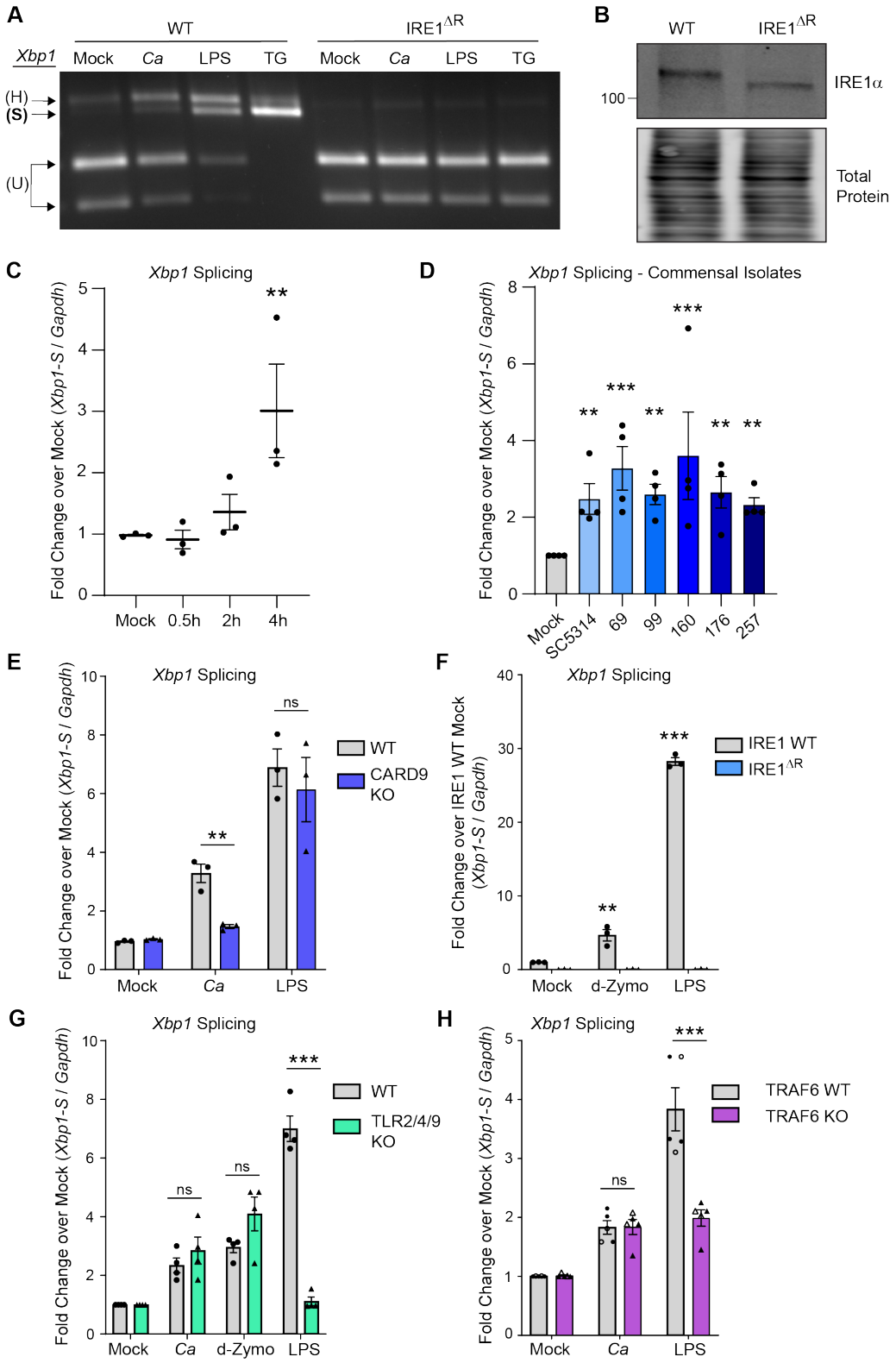

Figure 1: *C. albicans* infection results in activation of macrophage IRE1α. (A) iBMDM cell lines (WT or IRE1$^{\Delta R}$) were infected with *C. albicans* (MOI=1), treated with LPS (100 ng/mL), or thapsigargin (5 μM), or mock treated for 4 hours. *Xbp1* mRNA splicing was measured by semi-

quantitative RT-PCR amplification of the *Xbp1* transcript as a readout of IRE1α activity. **(B)** Immunoblot analysis of lysates from WT or IRE1$^{\Delta R}$ iBMDM cell lines to confirm IRE1α truncation in IRE1$^{\Delta R}$ cells resulting from removal of floxed exons 20 and 21. **(C)** Expression of the short isoform of *Xbp1* was measured using RT-qPCR over a timecourse following *C. albicans* infection of iBMDM (MOI=1). **(D)** Expression of the short isoform of *Xbp1* at 4 hours post-infection with commensal *C. albicans* isolates as well as the lab strain SC5314 (MOI=1) was measured using RT-qPCR. **(E)** Expression of the short isoform of *Xbp1* was measured using RT-qPCR at 4 hours following *C. albicans* infection (MOI=1) or LPS treatment (100 ng/mL) of WT or CARD9 KO iBMDM. **(F)** Expression of the short isoform of *Xbp1* was measured using RT-qPCR at 4 hours following *C. albicans* infection (MOI=1), depleted Zymosan treatment (d-Zymo; 100 µg/mL) to stimulate Dectin-1, or LPS treatment (100 ng/mL) of WT or IRE1$^{\Delta R}$ iBMDM. **(G)** Expression of the short isoform of *Xbp1* was measured using RT-qPCR at 4 hours following *C. albicans* infection (MOI=1), LPS treatment (100 ng/mL), or depleted Zymosan treatment (d-Zymosan; 100 µg/mL) of WT or TLR2/4/9 KO iBMDM. **(H)** Expression of the short isoform of *Xbp1* was measured using RT-qPCR at 4 hours following *C. albicans* infection or LPS treatment of two pairs of clonal iBMDM (WT or TRAF6 KO; MOI=1). Closed symbols are data from WT-1 and KO-1; open symbols are data from WT-2 and KO-2. Data are representative of 3-4 individual experiments. Graphs show the mean ± SEM of biological replicates (C-H). *$p < 0.05$, **$p < 0.01$, ***$p < 0.005$ by 2-way ANOVA of log-transformed data with Sidak's multiple comparisons test. ns, not significant.

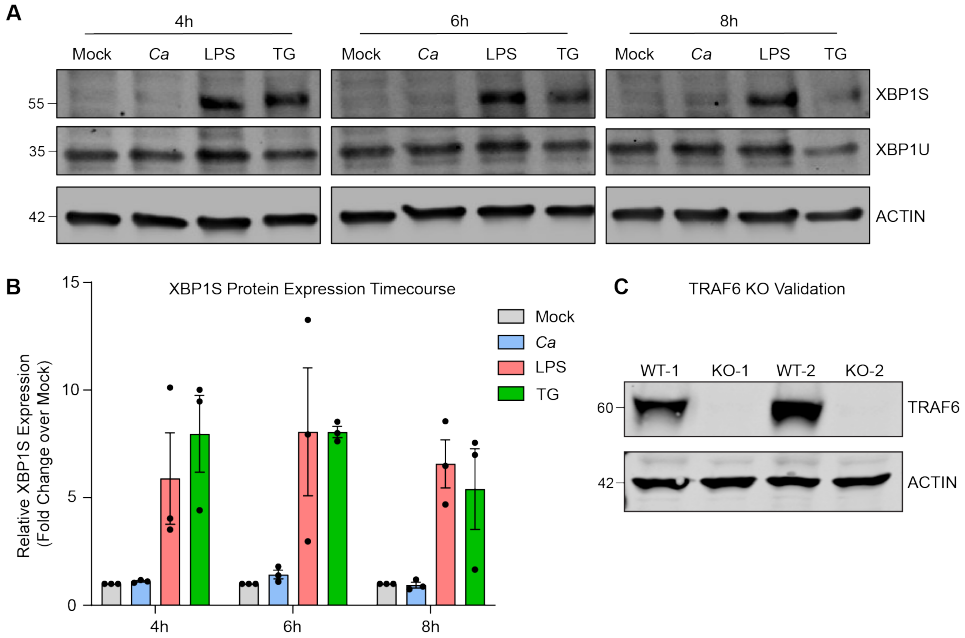

Figure S1: Related to Figure 1. (A) Immunoblot analysis of XBP1S and XBP1U expression from WT iBMDM lysates following infection with *C. albicans* (MOI=1), or treatment with positive controls

204 LPS (100 ng/mL) or thapsigargin (5 μM). **(B)** Quantification of 3 independent experiments, as
205 shown in (A). **(C)** Immunoblotting validation of clonal TRAF6 WT controls (WT-1 and WT-2) and
206 TRAF6 knockout iBMDM (KO-1 and KO-2).
207
208 **PRR-mediated activation of IRE1α occurs independently of misfolded protein stress.**
209 A potential mechanism for CLR-mediated IRE1α activation is by overwhelming protein
210 folding capacity of the ER due to increased cytokine production, leading to protein misfolding and
211 thus IRE1α activation. To test this hypothesis and determine whether new gene synthesis is
212 required for IRE1α activation during *C. albicans* infection, we inhibited transcription or translation
213 during infection with *C. albicans* or during treatment with thapsigargin. Surprisingly, neither
214 inhibition of transcription nor translation, using actinomycin D or cycloheximide treatment,
215 respectively, inhibited *Xbp1* splicing during *C. albicans* infection (Fig. 2A-B). Translation inhibition
216 using cycloheximide was sufficient to alleviate *Xbp1* splicing specifically in response to
217 thapsigargin, likely by reducing the nascent protein folding burden (Fig. 2B). These data indicate
218 that new gene synthesis does not contribute to IRE1α activation during *C. albicans* infection, and
219 presented the intriguing possibility that *C. albicans* infection does not induce unfolded proteins.
220 Indeed, this possibility has been suggested for TLR-driven IRE1α activation, but was not
221 previously directly tested[6,21]. To specifically test this, we measured whether misfolded proteins
222 accumulate during PRR-mediated activation of IRE1α by either *C. albicans* infection or LPS
223 treatment. Thioflavin T (ThT) is widely used to detect protein misfolding, as it exhibits increased
224 fluorescence in the presence of misfolded proteins[55]. While ThT intensity showed an expected
225 increase at 2 hours-post thapsigargin treatment, neither *C. albicans* infection nor LPS treatment
226 increased ThT intensity over mock treatment (Fig. 2C-D). Further, neither *C. albicans* infection
227 nor LPS treatment led to increased ThT intensity at 4 hpi, suggesting IRE1α activation occurs
228 without accumulation of misfolded proteins during these responses (Fig. 2E). Even at 8 hpi, *C.*
229 *albicans* infection did not induce protein misfolding (Fig. 2F). While LPS treatment did lead to
230 increased protein misfolding at 8 hours post-treatment (Fig. 2F), this occurred after the robust
231 IRE1α activation observed at 4 hours post-treatment (Fig. 1A). Finally, we measured induction of
232 UPR-responsive genes by RT-qPCR in response to *C. albicans* infection, LPS and depleted
233 zymosan treatment, or thapsigargin treatment (Fig. 2G-H). *C. albicans* infection and depleted
234 zymosan treatment did not lead to induction of UPR-responsive genes (*Ddit3*, *Grp78*, *Grp94*, and
235 total *Xbp1*) at 4 or 6 hours. Similarly, LPS treatment did not lead to global induction of UPR-
236 responsive genes, and only led to significant induction of *Grp78* at 4 hours and *Xbp1-T* at 6 hours.
237 Conversely, thapsigargin treatment triggered induction of all of these genes at both 4 and 6 hours

238 post-treatment, as expected (Fig. 2G-H). Together, these data suggest that while protein
239 misfolding can occur in response to microbial stimuli, it is not needed to trigger IRE1α activation
240 during innate immune responses, and points to a non-canonical mode of IRE1α activation during
241 infection.
242
243

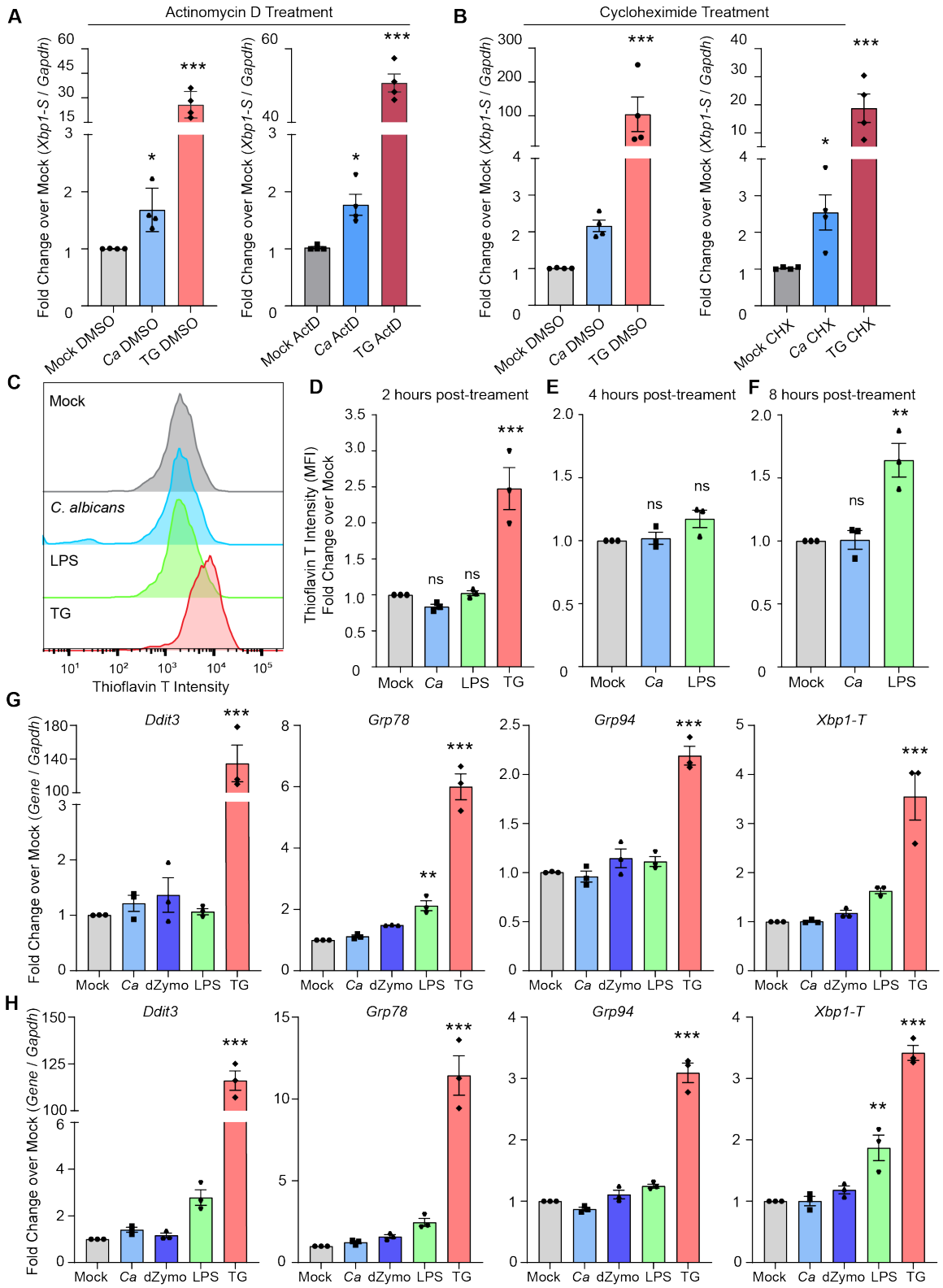

Figure 2: PRR-mediated activation of IRE1α occurs independently of misfolded protein stress. (A-B) Expression of the short isoform of *Xbp1* was measured using RT-qPCR following

247 *C. albicans* infection (MOI=1) of iBMDM or treatment with thapsigargin (TG; 5 μM) as a control,
248 compared to mock treatment. Actinomycin D (ActD; 20 μM) was used to inhibit new transcription
249 during treatments (A), and cycloheximide (CHX; 10 μM) was used to inhibit translation during
250 treatments (B), and relative fold changes were measured over matched mock samples. **(C)**
251 Representative graphs showing fluorescence intensity of Thioflavin T (ThT) measured by flow
252 cytometry to quantify protein misfolding in iBMDM following infection by *C. albicans* (MOI=1), or
253 treatment with LPS (100 ng/mL) or thapsigargin (TG; 5 μM) as a positive control. **(D-F)**
254 Quantification of ThT fluorescence intensity at 2 hours (D), 4 hours (E), or 8 hours post-indicated
255 treatment, shown as fold change over mock. **(G-H)** Expression of UPR-responsive genes was
256 measured using RT-qPCR at 4 hours (G) or 6 hours (H) following *C. albicans* infection (MOI=1),
257 depleted Zymosan treatment (d-Zymosan; 100 μg/mL), LPS treatment (100 ng/mL), or
258 thapsigargin treatment (TG; 5 μM). Graphs show the mean ± SEM of biological replicates. *$p <$
259 0.05, **$p < 0.01$, ***$p < 0.005$ by 2-way ANOVA with Sidak's multiple comparisons test of log-
260 transformed data (A, B), one-way ANOVA with Tukey's multiple comparisons test (D-F), or one-
261 way ANOVA with Dunnett's multiple comparisons test (G-H).
262
263 **IRE1α promotes phagosome maturation during C. albicans infection.**
264 To explore the potential roles of IRE1a in macrophage antifungal functions, we first tested
265 the ability of IRE1 WT and IRE1$^{\Delta R}$ macrophages to ingest *C. albicans* through phagocytosis.
266 Interestingly, IRE1$^{\Delta R}$ macrophages showed increased efficiency of *C. albicans* phagocytosis (Fig.
267 3A-B). Following phagocytosis of large particles, the ER is thought to regulate phagosome
268 maturation through poorly understood mechanisms[56]. Importantly, phagosome maturation is
269 required for containment of *C. albicans* hyphae within the phagosome, as lysosome fusion allows
270 membrane donation to support expansion of the phagosome[44]. Therefore, we next tested whether
271 IRE1$^{\Delta R}$ macrophages showed impaired phagosome maturation during *C. albicans* infection by
272 measuring recruitment of the lysosomal protein LAMP1 to the phagosome containing *C. albicans*
273 (Fig. 3C-D). IRE1 WT macrophages recruited LAMP1 to the phagosome by 2 hpi, but IRE1$^{\Delta R}$
274 macrophages infected with *C. albicans* failed to efficiently recruit LAMP1 to the phagosome (Fig.
275 3C-D). However, overall lysosome biogenesis did not appear to be impaired in IRE1$^{\Delta R}$
276 macrophages, as labeling acidic cellular compartments with LysoSensor Blue/Yellow dye showed
277 IRE1$^{\Delta R}$ macrophages had similar acidity as IRE1 WT macrophages, and *C. albicans* infection or
278 ammonium chloride treatment led to the expected alkalinization of both cell lines [46,57–59] (Fig. 3E).
279 These data suggest that IRE1α activity is specifically required for efficient phagolysosomal fusion
280 during *C. albicans* infection.

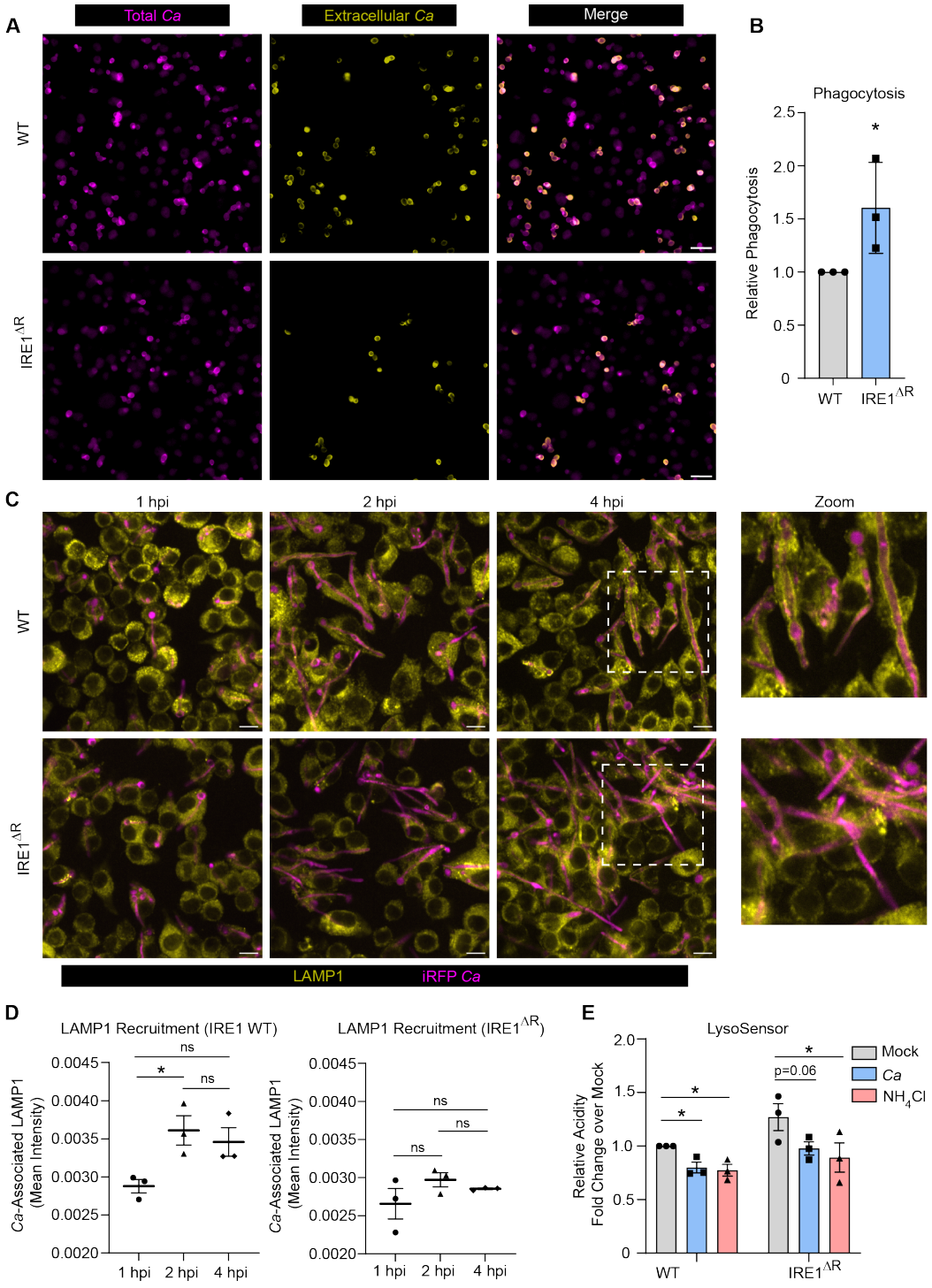

Figure 3: IRE1α promotes phagosome maturation during *C. albicans* infection. (A) Representative phagocytosis assay micrographs show total *C. albicans* (intracellular and extracellular; magenta) and extracellular *C. albicans* (yellow) following 30 minutes of phagocytosis by iBMDM (IRE1 WT or IRE1$^{\Delta R}$). Scale bar 10 μm. **(B)** Quantification of 3 independent phagocytosis experiments. Relative phagocytosis was calculated as fold change over IRE1 WT.

287 **(C)** Representative images showing LAMP1 (yellow) recruitment to phagosomes containing iRFP-
288 expressing *C. albicans* (magenta) in IRE1 WT or IRE1$^{\Delta R}$ iBMDM at indicated times post-infection.
289 **(D)** Quantification of LAMP1 recruitment to phagosomes containing *C. albicans* in IRE1 WT or
290 IRE1$^{\Delta R}$ iBMDM, as measured by LAMP1 mean fluorescence intensity associated with *C. albicans*-
291 expressed iRFP. **(E)** The relative acidity of IRE1 WT or IRE1$^{\Delta R}$ iBMDM following infection with *C.*
292 *albicans* or treatment with NH_4Cl as a control, shown as the relative ratio of LysoSensor intensity
293 at acidic (Excitation 384 nm, Emission 540 nm) and basic (Excitation 329 nm, Emission 440 nm)
294 conditions. Values are the mean ± SEM from 3 biological replicates. *$p < 0.05$, **$p < 0.01$, *** $p <$
295 0.001, by unpaired Student's t-test (B) or one-way ANOVA with Tukey's multiple comparisons test
296 (D, E).
297
298 **IRE1α promotes phagosomal calcium flux necessary for phagosome maturation.**
299 To understand of the role of IRE1α in phagosome maturation, we investigated its impact
300 on gene expression during *C. albicans* infection or mock treatment using RNA sequencing.
301 Despite not observing robust XBP1S induction during *C. albicans* infection (Fig. S1), we reasoned
302 that IRE1α activity could modulate gene expression by XBP1S-independent mechanisms, such
303 as cleavage of other transcripts or microRNAs[60–62], or interaction with ER-localized RNA species
304 under homeostatic or ER stress conditions[63]. As expected, we found many differentially regulated
305 genes in IRE1$^{\Delta R}$ macrophages during *C. albicans* infection (Fig. S2A; Table S1.1) compared with
306 WT macrophages at 4 hpi. Importantly, the IRE1$^{\Delta R}$ macrophages had broadly similar expression
307 of ER stress-related genes as WT control macrophages, suggesting that lack of IRE1α does not
308 result in chronic ER stress during infection (Fig. S2B). Interestingly, gene ontology analysis
309 revealed that genes involved in endocytosis and calcium homeostasis were enriched among
310 downregulated genes in IRE1$^{\Delta R}$ macrophages (Table S1.2). These included genes involved in ER
311 homeostasis (*Kctd17*, *Atp2a3*, *Gramd2*)[64–66], as well as the major lysosome calcium channels
312 *Mcoln1* and *Mcoln3*[67] (Fig. S2C). However, the expression of genes involved in general cellular
313 calcium uptake and homeostasis, such as *Calm1*, *Calr*, *Stim1*, *Orai1-3*, and *Ryr1* and *Ryr3* was
314 similar in WT and IRE1$^{\Delta R}$ macrophages (Fig. S2C). Therefore, we hypothesized that organellar
315 calcium signaling may be specifically impaired in IRE1$^{\Delta R}$ macrophages. Calcium flux regulates
316 phagosome formation and maturation[68] and is required for lysosome recruitment to the
317 phagosome during *C. albicans* infection[44]. We investigated whether calcium flux is perturbed in
318 IRE1$^{\Delta R}$ macrophages during phagocytosis of *C. albicans* using the fluorescent calcium ion
319 indicator Fluo4-AM. In WT macrophages, calcium flux was observed during macrophage-*C.*
320 *albicans* interactions and during phagocytosis of *C. albicans* (Supplemental Movie 1, Fig. 4A). At

321 baseline, WT and IRE1$^{\Delta R}$ macrophages showed similar Fluo4 fluorescence intensity, suggesting
322 calcium stores are not depleted in IRE1$^{\Delta R}$ macrophages (Fig. 4B). Additionally, we measured
323 cellular calcium flux per cell in WT and IRE1$^{\Delta R}$ macrophages following *C. albicans* infection
324 (Supplemental Figure 3A). Cellular calcium flux was comparable between WT and IRE1$^{\Delta R}$
325 macrophages, as similar frequency of cellular calcium flux was observed (Fig. 4C), as well as
326 similar 'excitability' of macrophages during *C. albicans* infection (Fig. 4D). However, shortly after
327 phagocytosis, phagosomal calcium influx was frequently observed in WT macrophages
328 (Supplemental Movie 1, Fig. 4A), seen as a clear but transient ring around the engulfed yeast.
329 However, phagosomal calcium flux was rarely observed in IRE1$^{\Delta R}$ macrophages after
330 phagocytosis of *C. albicans* (Supplemental Movie 2, Fig. 4E). Indeed, quantification of
331 phagosomal calcium flux at 20 minutes post-infection in WT macrophages revealed that roughly
332 half of macrophages that had phagocytosed *C. albicans* had active phagosomal calcium flux, with
333 phagosomal intensity above that of the cytosol, whereas less than 20 percent of IRE1$^{\Delta R}$
334 macrophages showed phagosomal calcium flux (Fig. 4F). Additionally, the fluorescence intensity
335 of the *C. albicans* phagosome relative to the cytosol was higher in WT macrophages than in
336 IRE1$^{\Delta R}$ macrophages (Fig. 4G). Together, these data suggest that phagosomal calcium flux is
337 specifically impaired in IRE1$^{\Delta R}$ macrophages, possibly due to defective expression of calcium
338 signaling-related genes. Previous work showed that phagosome-derived calcium is required for
339 lysosome recruitment during *C. albicans* infection, and that calcium chelation disrupts phagosome
340 maturation[44]. Therefore, to test the hypothesis that calcium flux is required for maturation of *C.*
341 *albicans*-containing phagosomes, we treated macrophages with a cell permeable calcium
342 chelator, BAPTA-AM, during *C. albicans* infection. BAPTA-AM treatment impaired phagosome
343 maturation in WT macrophages, while defective phagosome maturation observed in IRE1$^{\Delta R}$
344 macrophages was not further impacted by BAPTA-AM treatment (Fig. 4H). These data suggest
345 that defective phagosomal calcium flux in IRE1$^{\Delta R}$ macrophages perturbs phagosome maturation.

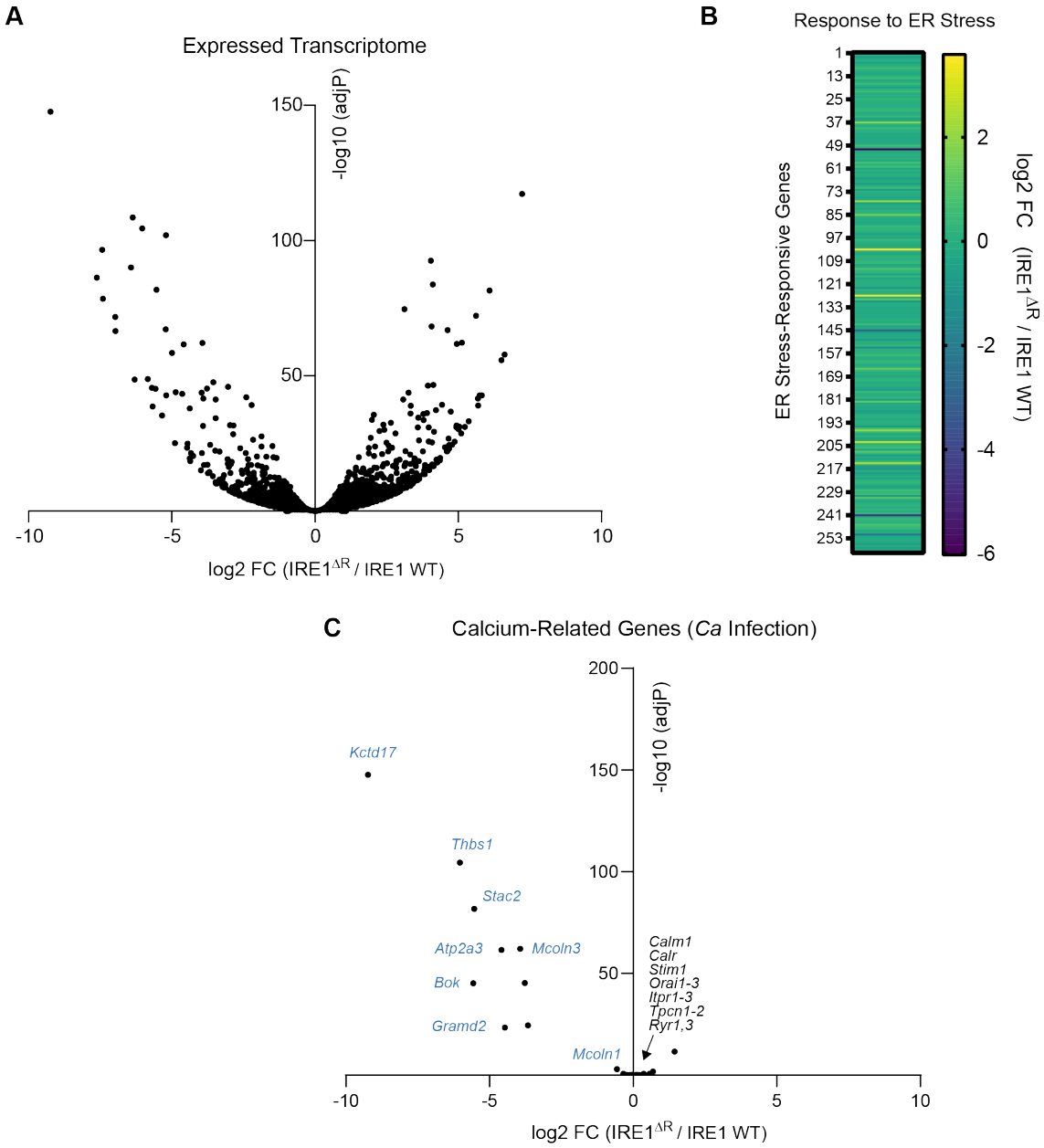

Supplemental Figure 2: IRE1α regulates macrophage gene expression. (A) Volcano plot of the effect of IRE1α activity ablation on the expressed transcriptome (IRE1$^{\Delta R}$ / IRE1 WT) of iBMDM, revealed by RNA-seq. **(B)** Heatmap of differential gene expression in IRE1$^{\Delta R}$ iBMDM of genes in the GO category "Response to ER stress", showing that IRE1$^{\Delta R}$ macrophages do not have a chronic ER stress signature. **(C)** Heatmap of downregulated genes involved in organelle calcium homeostasis (blue text) in IRE1$^{\Delta R}$ iBMDM, and major calcium homeostasis regulators (black text) whose expression is not impacted.

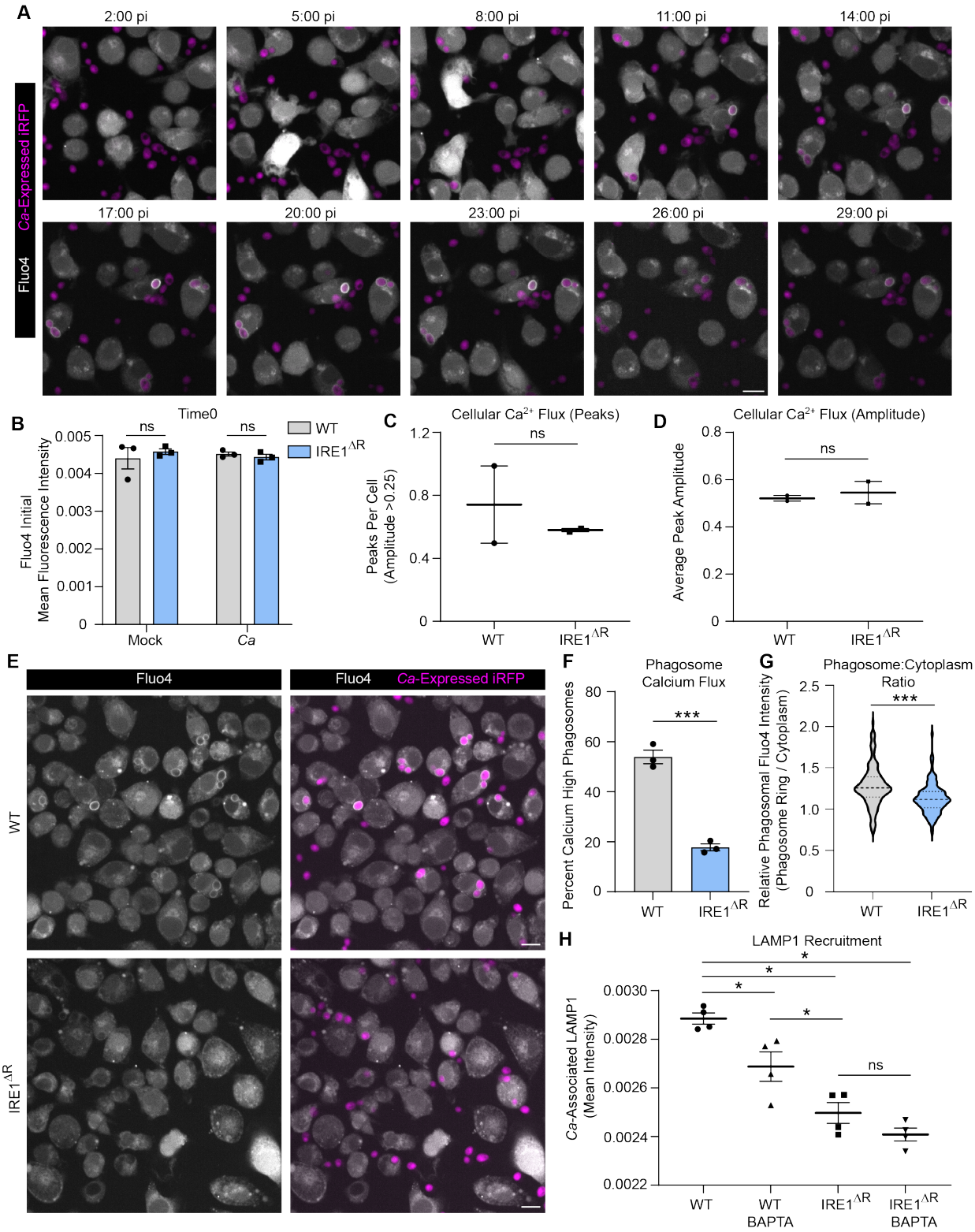

Figure 4: IRE1α promotes phagosomal calcium flux necessary for phagosome maturation. (**A**) Representative micrographs from timelapse imaging of Fluo4 during *C. albicans* infection of WT iBMDM. Scale bar 10 μm. **(B)** Mean fluorescence intensity of Fluo4 at time 0, or the beginning

358 of live imaging, in WT or IRE1$^{\Delta R}$ iBMDM. **(C-D)** Analysis of cellular calcium flux of WT or IRE1$^{\Delta R}$
359 iBMDM during early interactions with *C. albicans*. Graphs show the number of peaks per cell,
360 defined as ≥0.25 increase in normalized Fluo4 fluorescence (C), or the average amplitude of
361 peaks (D). **(E)** Representative micrographs of WT or IRE1$^{\Delta R}$ iBMDM following phagocytosis of *C.*
362 *albicans* (20 mins post-infection; MOI 2) showing early cellular calcium flux, and influx of calcium
363 specifically in the phagosome following phagocytosis of *C. albicans*. Scale bar 10 μm. **(F)**
364 Quantification of calcium-high phagosomes, defined by a 1.25-fold increase of the mean
365 fluorescence intensity of the cell (20 mins post-infection; MOI 2). **(G)** Violin plot of the ratio of
366 phagosomal to cytosolic mean fluorescence intensity of Fluo4 (20 mins post-infection; MOI 2). **(H)**
367 Quantification of LAMP1 recruitment to phagosomes containing *C. albicans* in IRE1 WT or IRE1$^{\Delta R}$
368 iBMDM with or without treatment of BAPTA-AM, a cell-permeable calcium chelator, as measured
369 by LAMP1 mean fluorescence intensity associated with *C. albicans*-expressed iRFP. Values are
370 the mean ± SEM from 2-4 biological replicates, as indicated by data points. *$p < 0.05$, **$p < 0.01$,
371 *** $p < 0.001$, by unpaired Student's t-test (B-D, F, G) or one-way ANOVA with Tukey's multiple
372 comparisons test (H).
373

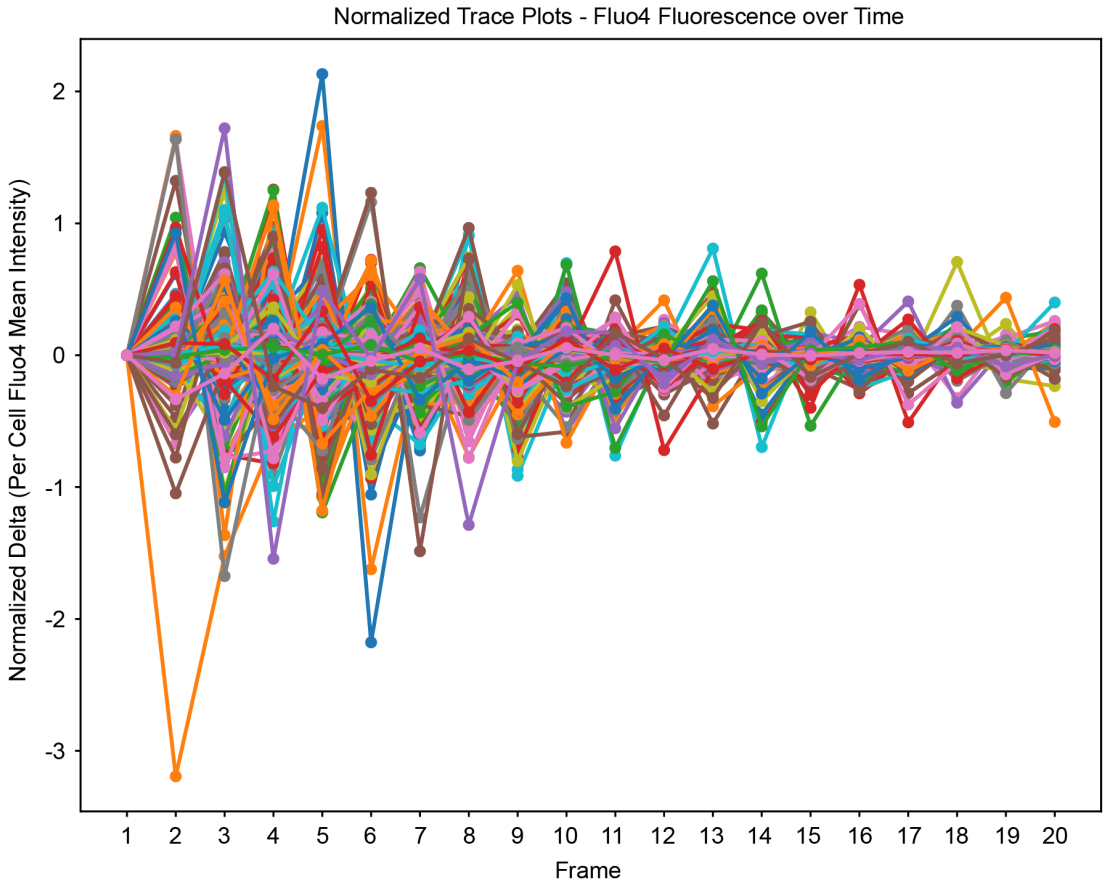

374

375 **Supplemental Figure 3: Related to Figure 4.** Representative trace plots of cellular Fluo4
376 intensity in individual cells tracked over time for quantification of cellular calcium flux, as shown in
377 Figure 4C-D.
378
379 **IRE1α promotes phagosome integrity and macrophage fungistatic activity.**
380 As lysosome recruitment maintains the integrity of the expanding phagosome during *C.*
381 *albicans* infection[44], we reasoned that *C. albicans* may escape the phagosome more readily in
382 IRE1$^{\Delta R}$ macrophages. To test this, we used a previously-established pulse-chase assay to
383 measure phagosome leakage in which endosomes are pre-labeled with sulforhodamine B (SRB),
384 allowing fusion with *C. albicans* containing phagosomes and monitoring of phagosome rupture[44,69]
385 (Fig. 5A). Measuring SRB association with the *C. albicans*-containing phagosome over time
386 revealed that SRB was lost from the phagosome more rapidly in IRE1$^{\Delta R}$ macrophages, supporting
387 the hypothesis that IRE1α activity contributes to maintenance of the *C. albicans*-containing
388 phagosome by promoting phagolysosomal fusion (Fig. 5B). As the phagolysosomal environment
389 restricts *C. albicans* hyphal growth[70], we also measured hyphal growth over time in WT and
390 IRE1$^{\Delta R}$ macrophages and found that *C. albicans* hyphal growth is increased at 4 hpi in IRE1$^{\Delta R}$
391 macrophages (Fig. 5C), demonstrating that IRE1α activity promotes the fungistatic activity of
392 macrophages. Phagosome rupture during *C. albicans* infection has been associated with
393 macrophage proinflammatory cytokine production[37,40,44,71]. Therefore, we tested secretion of IL-
394 1β, TNF, and IL-6 from WT and IRE1$^{\Delta R}$ macrophages after LPS priming and *C. albicans* infection
395 (Fig. 5D-F). Consistent with increased phagosome rupture observed in IRE1$^{\Delta R}$ macrophages, we
396 also saw increased supernatant IL-1β and TNF levels, while IL-6 levels were unaffected (Fig. 5D-
397 F). Together, these data suggest that IRE1α activity promotes phagosome integrity and
398 macrophage fungistatic activity during *C. albicans* infection.
399

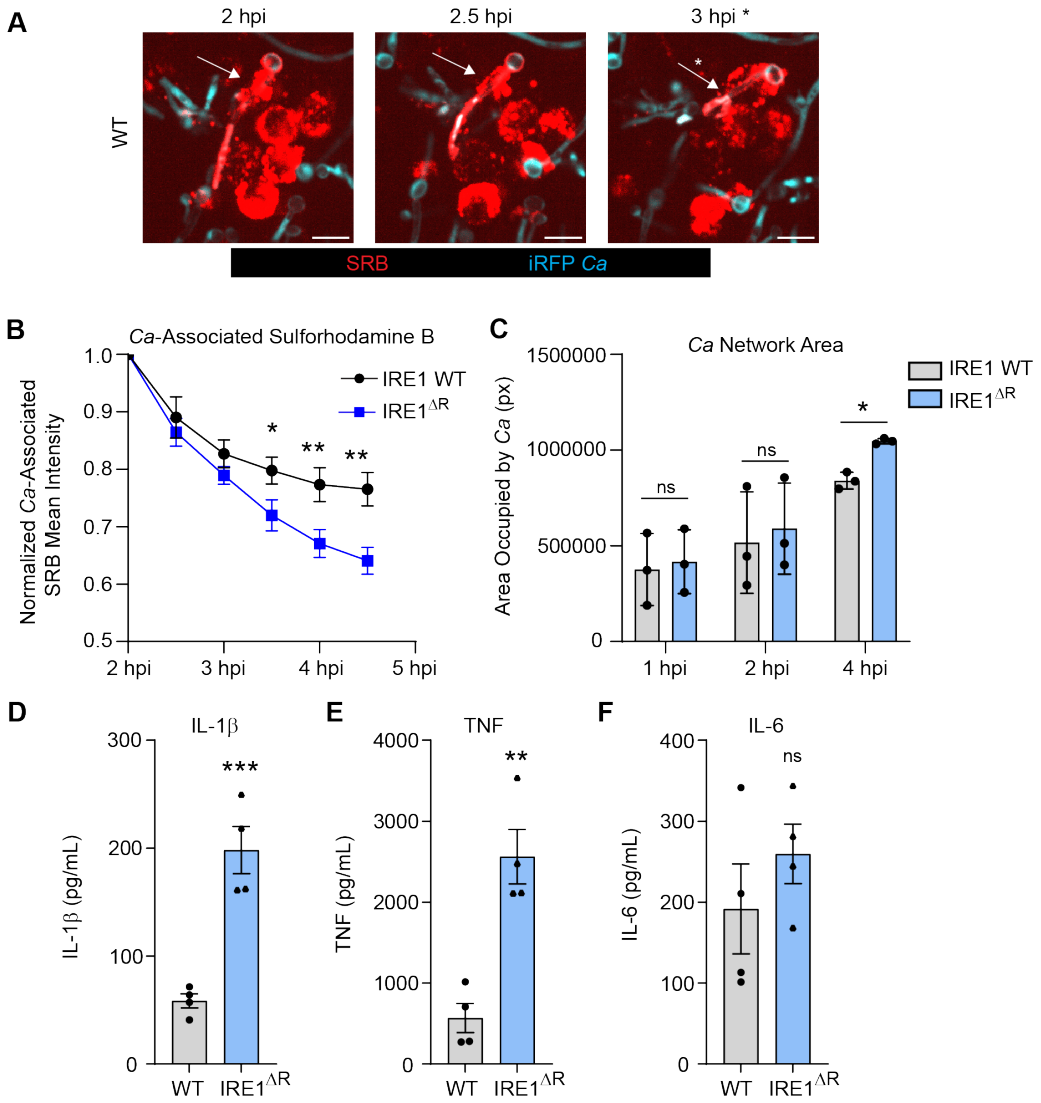

Figure 5: IRE1α promotes phagosome integrity and macrophage fungistatic activity. **(A)** Representative images of SRB recruitment to the phagosome containing *C. albicans*, indicated by white arrows, and loss of SRB association following phagosomal rupture at 3 hpi, indicated by white asterisk. Scale bar 10 µm. **(B)** Quantification of 3 independent experiments measuring the loss of SRB from *C. albicans* over time in IRE1 WT or IRE1$^{\Delta R}$ iBMDM. **(C)** Quantification of the area occupied (pixels) by *C. albicans* hyphae at 1, 2, and 4 hpi in IRE1 WT or IRE1$^{\Delta R}$ iBMDM. **(D-F)** Expression of proinflammatory cytokines (IL-1β (D), TNF (E), and IL-6 (F)) were measured by ELISA following 3 h of LPS priming and 5 h of *C. albicans* infection (MOI=1) in IRE1 WT and IRE1$^{\Delta R}$ iBMDM. Graphs show the mean ± SEM of 3-4 biological replicates. *$p < 0.05$, **$p < 0.01$, *** $p < 0.001$ by unpaired Student's t test (B, D-F), or one-way ANOVA with Tukey's multiple comparisons test (C).

413 **IRE1α promotes macrophage fungicidal activity.**

414 Escape from the phagosome likely allows *C. albicans* to evade fungicidal effectors in
415 addition to allowing for more rapid growth. To determine whether IRE1α contributes to
416 macrophage fungicidal activity, we measured the ability of IRE1α WT and IRE1$^{\Delta R}$ macrophages
417 to kill phagocytosed *C. albicans*, using a dual fluorescence assay in which iRFP-expressing *C.*
418 *albicans* is pre-labeled with calcofluor white (CFW) prior to macrophage infection (Fig. 6A). Live
419 *C. albicans* express iRFP and are CFW labeled (iRFP^{+} CFW^{+}), while killed *C. albicans* lose iRFP
420 fluorescence but can be identified by CFW labeling (iRFP^{-} CFW^{+}). Using this assay, we found that
421 IRE1$^{\Delta R}$ macrophages were defective at killing phagocytosed *C. albicans*, demonstrating that
422 IRE1α activity contributes to the fungicidal activity of macrophages (Fig. 6B).

423 To determine whether failure to recruit lysosomes to the phagosome is responsible for the
424 fungicidal defect observed in IRE1$^{\Delta R}$ macrophages, we tested the effect of Bafilomycin A (BafA),
425 which inhibits vacuolar ATPase activity and thus phagosome-lysosome fusion, on the ability of
426 IRE1 WT and IRE1$^{\Delta R}$ macrophages to kill *C. albicans* (Fig. 6C). BafA treatment suppressed the
427 fungicidal activity of both IRE1 WT and IRE1$^{\Delta R}$ macrophages, reinforcing the importance of
428 phagolysosomal fusion for killing of *C. albicans*. Additionally, BafA treatment ablated the
429 difference between IRE1 WT and IRE1$^{\Delta R}$ macrophages in fungicidal capacity, demonstrating that
430 defective phagolysosomal fusion in IRE1$^{\Delta R}$ macrophages is responsible for their compromised
431 fungicidal activity (Fig. 6C). Together, these data support a model in which IRE1α activity supports
432 phagolysosomal fusion during *C. albicans* infection of macrophages to maintain phagosome
433 integrity and allow killing of ingested *C. albicans*.
434
435
436

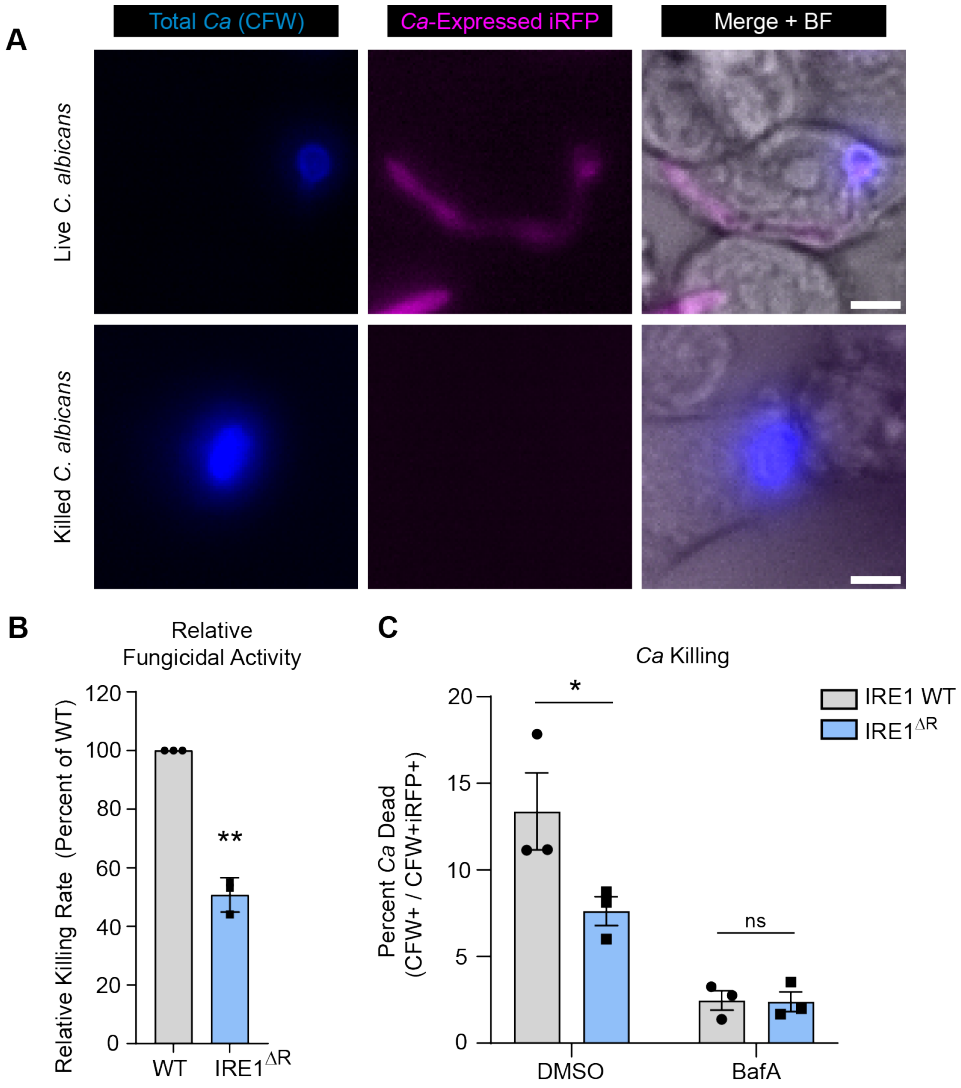

Figure 6: IRE1α promotes macrophage fungicidal activity. (A) Representative micrographs of live intracellular *C. albicans* and killed intracellular *C. albicans* within IRE1 WT iBMDM at 7 hpi. Endogenous expression of iRFP by *C. albicans* indicates viability (CFW+ iRFP+); loss of iRFP expression indicates killed *C. albicans* (CFW+ iRFP-). Scale bar 5 μm. **(B)** Quantification of 3 independent *C. albicans* killing experiments (CFW+ iRFP- / CFW+ iRFP+), relative to WT. **(C)** Graphs show the mean ± SEM of 3 biological replicates. *$p < 0.05$, **$p < 0.01$, by unpaired Student's t test (B), or two-way ANOVA with Tukey's multiple comparisons test (C).

IRE1α regulates cytokine production and phagocyte fungicidal activity *in vivo*.

449 Our *in vitro* assays allowed in-depth interrogation of the role of IRE1α in interactions
450 between *C. albicans* and bone marrow-derived macrophages. To examine the impact of IRE1α
451 during systemic *C. albicans* infection *in vivo*, we utilized LysM-Cre to delete IRE1α activity in
452 macrophages and neutrophils in mice (IRE1$^{fl/fl}$ LysM^{Cre}), followed by systemic infection with *C.*
453 *albicans* expressing iRFP for 24 hours. Previous work demonstrated that the IRE1α-XBP1S axis
454 in neutrophils drives fatal immunopathology starting at 5 days post-systemic *C. albicans*
455 infection[14]. However, we found that female IRE1$^{fl/fl}$ LysM^{Cre} mice had higher levels of serum
456 cytokines such as IL-1Ra, TNF, and IL-6 than littermate controls (IRE1$^{fl/fl}$) at 24 hpi (Fig. 7A).
457 These data are in agreement with the suppressive effect of IRE1α activity on cytokine production
458 in macrophages observed in our *in vitro* assays (Fig. 5A). Interestingly, these increased cytokine
459 levels were observed specifically in female mice, as male mice exhibited generally similar cytokine
460 levels to littermate controls (Fig. 7B), suggesting sex-specific roles for IRE1α during *C. albicans*
461 infection. Additionally, we determined whether IRE1α supports the fungicidal activity of
462 phagocytes *in vivo* using an immunofluorescence assay with dissociated kidney samples from
463 IRE1$^{fl/fl}$ LysM^{Cre} mice compared to IRE1$^{fl/fl}$ controls. For this assay, *C. albicans* viability in myeloid
464 cells was measured using an anti-*Candida* antibody to identify total *C. albicans* and iRFP to
465 indicate viability, as well as anti-CD11b to identify leukocytes that had phagocytosed *C. albicans*
466 within the kidney (Fig. 7C). Quantification of *C. albicans* viability within the kidney tissue revealed
467 that while overall *C. albicans* viability in the kidney tissue was not different between IRE1$^{fl/fl}$
468 LysM^{Cre} mice and IRE1 $^{fl/fl}$ control mice (Fig. 7D), *C. albicans* killing by phagocytic cells was less
469 effective in mice lacking IRE1α activity (Fig. 7E), and this difference in killing efficacy between
470 IRE1$^{fl/fl}$ and IRE1$^{fl/fl}$ LysM^{Cre} phagocytes appeared to be exacerbated in female mice (Fig. 7F).
471 These data suggest that IRE1α supports the fungicidal activity of phagocytic cells *in vivo*, in
472 agreement with our *in vitro* data, and interestingly suggest a sex-specific role for IRE1α in
473 coordinating cytokine responses and controlling fungal infection in female mice. Together, these
474 data establish a role for IRE1α in suppressing serum cytokine production and the fungicidal
475 activity of phagocytes *in vivo*.

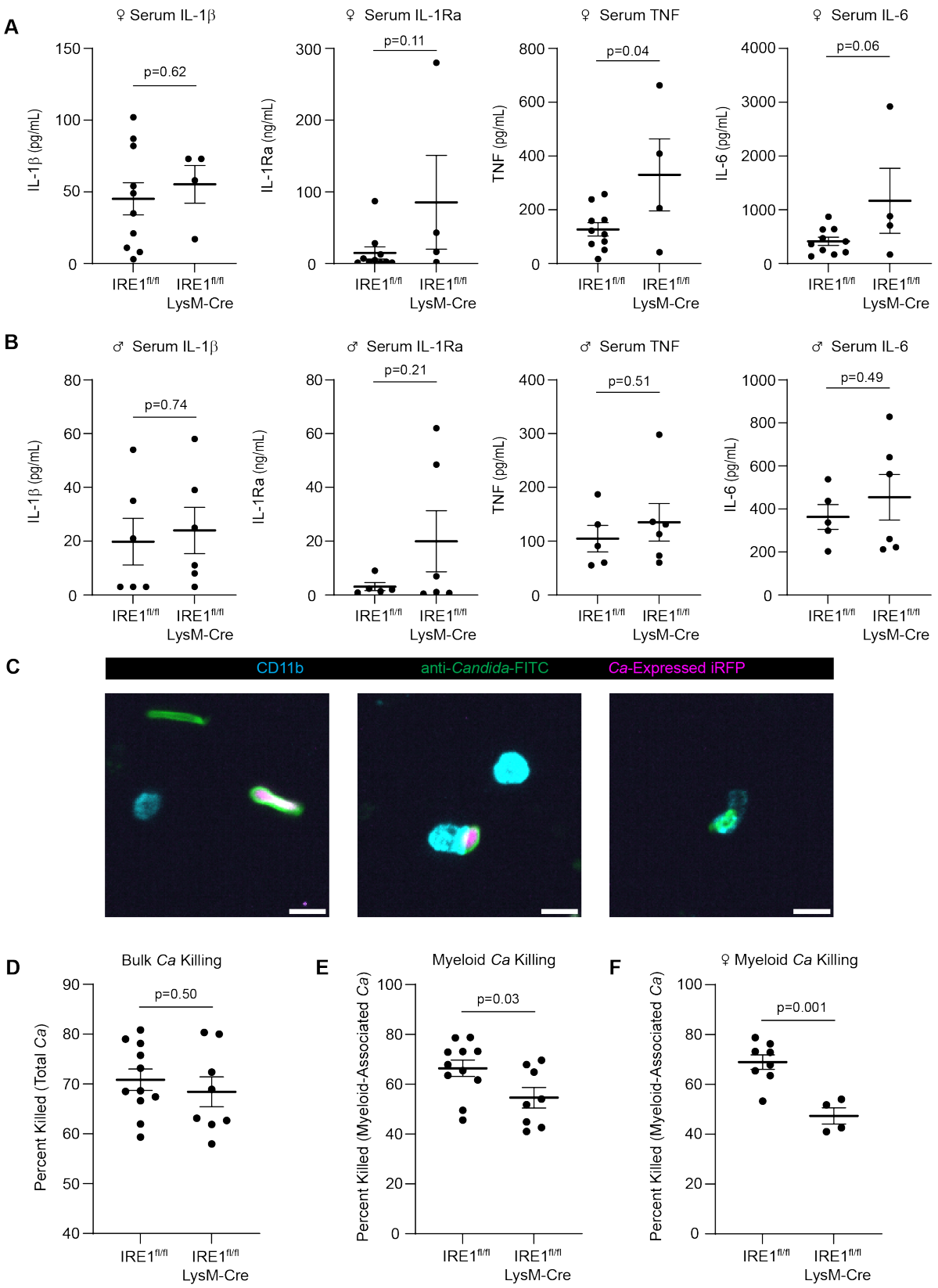
A
♀ Serum IL-1β
IL-1β (pg/mL)
p=0.62
♀ Serum IL-1Ra
IL-1Ra (ng/mL)
p=0.11
♀ Serum TNF
TNF (pg/mL)
p=0.04
♀ Serum IL-6
IL-6 (pg/mL)
p=0.06
IRE1fl/fl
IRE1fl/fl LysM-Cre
B
♂ Serum IL-1β
p=0.74
♂ Serum IL-1Ra
p=0.21
♂ Serum TNF
p=0.51
♂ Serum IL-6
p=0.49
C
CD11b
anti-Candida-FITC
Ca-Expressed iRFP
D
Bulk Ca Killing
Percent Killed (Total Ca)
p=0.50
E
Myeloid Ca Killing
Percent Killed (Myeloid-Associated Ca)
p=0.03
F
♀ Myeloid Ca Killing
p=0.001

476

477 **Figure 7:** IRE1α activity in myeloid cells regulates cytokine levels and phagocyte fungicidal
478 activity *in vivo*. **(A-B)** ELISA data from mouse serum 24 hours post-systemic *C. albicans* infection
479 in female (A) or male (B) mice. Mice were intravenously infected with 10^6 CFU and serum was
480 collected through cardiac puncture. **(C)** Representative micrographs of *C. albicans* in dissociated
481 kidney cells showing total *C. albicans* (anti-*Candida*-FITC+) in green, live *C. albicans* (anti-
482 *Candida*-FITC+ *C. albicans*-expressed iRFP+), and CD11b positive cells to identify host
483 leukocytes. Images show non-myeloid-associated live and dead *C. albicans* (left), myeloid-
484 associated live *C. albicans* (middle), and myeloid-associated killed *C. albicans* (right). Scale bar
485 10 μm. **(D-F)** The percent of *C. albicans* killed was quantified in the kidney tissue (D), in myeloid
486 cells from male and female mice (E), or in myeloid cells from female mice only (F). Graphs show
487 the mean±SEM of data from individual mice. P values determined by unpaired Student's t test.
488
489
490 **Discussion**
491 Cell and organelle stress responses are crucial regulators of innate immunity and infection
492 outcomes during bacterial and viral infection[1,2], however, the role of these stress responses in
493 antifungal innate immunity have not been explored in depth. Here, we show that *C. albicans*
494 infection of macrophages results in activation of the IRE1α branch of the mammalian ER stress
495 response. This activation is not dependent on misfolded protein stress, but instead requires
496 signaling through the CLR pathway. Interestingly, macrophages lacking IRE1α activity have
497 impaired fungicidal activity due to inefficient lysosome recruitment to the phagosome containing
498 *C. albicans*, allowing phagosomal escape by *C. albicans* and likely evasion of fungicidal effectors.
499 Together, these results demonstrate roles for IRE1α in the antifungal responses of macrophages.
500 IRE1α is known to be activated by bacterial and viral infections, but the mechanisms
501 driving its activation are incompletely understood. While it has been suggested that innate
502 immune signaling may trigger IRE1α activation independently of misfolded protein stress, this
503 hypothesis had not been thoroughly tested. Here, we determined that CLR signaling through
504 CARD9 triggers IRE1α activation during *C. albicans* infection. Notably, measurable protein
505 misfolding did not precede IRE1α activation in response to either *C. albicans* infection or LPS
506 treatment, suggesting a potential protein misfolding-independent shared mechanism of IRE1α
507 activation downstream of innate immune signaling. However, neither TLR signaling nor TRAF6
508 activity were required for IRE1α activation during *C. albicans* infection, demonstrating that TLR
509 and CLR signaling activate IRE1α through distinct mechanisms and that *C. albicans* triggers non-
510 canonical activation of IRE1α.

511 A potential route of IRE1α activation in the absence of misfolded protein accumulation is
512 post-translational modification, such as ubiquitination or phosphorylation [21,72]. Ubiquitination of
513 IRE1α by E3 ubiquitin ligases such as TRAF6 and CHIP contribute to IRE1α activation in
514 response to LPS treatment or geldanamycin-induced ER stress, respectively[21,73]. However, we
515 found IRE1α activation is TRAF6-independent during *C. albicans* infection, suggesting an
516 alternative mechanism of activation. Additionally, the endonuclease activity of IRE1α depends on
517 its phosphorylation status, which is governed by its own kinase activity, or in certain contexts may
518 be triggered by other kinases[72]. We observed that CLR-mediated IRE1α activation required
519 CARD9 in response to *C. albicans*. CARD9 forms a complex with BCL10 and MALT1, resulting
520 in a filamentous scaffold for the assembly and activation of additional post-translational modifiers,
521 such as the kinase TAK1 and the E3 ubiquitin ligase TRAF2, which interacts with IRE1α but is
522 thought to act downstream of IRE1α[74]. Therefore, CARD9 activation could facilitate interaction of
523 IRE1α with a post-translational modifier to enable its activation. As CARD family proteins and
524 IRE1α have broad and overlapping functions in innate immune activation and immune cell
525 function[75,76], future work interrogating the molecular mechanisms by which CARD9 triggers IRE1α
526 activation will be of interest.
527 The convergence of TLR and CLR signaling on IRE1α activation in macrophages,
528 seemingly prior to accumulation of misfolded proteins, leads us to propose a model in which innate
529 immune signaling induces anticipatory activation of IRE1α. This may serve to increase the
530 secretory activity of macrophages prior to protein misfolding for efficient innate immune
531 responses. IRE1α activity is crucial for the maturation and function of highly secretory cell types,
532 such as plasma cells[77,78], pancreatic beta cells[79], macrophages[6,80], and T cells[81]. Additionally,
533 considering the broad roles of IRE1α and XBP1S in innate immunity, including cytokine
534 induction[6,10], metabolic plasticity[24], ROS production, and microbicidal activity[12,13], proactive
535 strategies for IRE1α activation prior to protein misfolding may be important for innate immune
536 regulation. Further elucidation of the mechanisms driving protein misfolding-independent IRE1α
537 activation will identify targets for tuning of IRE1α activity, with potential for therapeutic utility for
538 diseases in which aberrant IRE1α activity may contribute to disease progression, such as cancer
539 and obesity[82,83]. Exploration of other pathways that may trigger non-canonical activation of IRE1α
540 will help shape our understanding of IRE1α regulation.
541 When investigating the consequences of IRE1α activity during antifungal responses, we
542 found a novel regulatory function of IRE1α in promoting transient phagosomal calcium flux. Using
543 live imaging, we reveal transient phagosomal calcium influx during *C. albicans* infection that
544 occurs several minutes after phagocytosis and is promoted by IRE1α. Interestingly, as IRE1α-

545 dependent phagosomal calcium flux was observed within minutes of infection, this phenotype
546 may reflect basal functions of IRE1α activity, rather than CLR-mediated IRE1α activation. While
547 it has been previously shown that calcium flux is required for phagosome maturation during *C.*
548 *albicans* infection[44], and Candidalysin has been shown to induce cellular calcium flux in epithelial
549 cells[84], the transient accumulation of calcium in the *C. albicans* phagosome has not been
550 described previously. Moreover, the source of this calcium and the mechanism of its uptake into
551 the phagosome are not yet defined. Previous work has shown that IRE1α can be recruited to
552 pathogen-containing autophagosomes[85], and ER-phagosome contact sites can regulate
553 phagolysosomal fusion through calcium signaling[86]. Interestingly, IRE1α can function as a
554 scaffold at ER-mitochondria contact sites, allowing mitochondrial calcium uptake and regulation
555 of cellular metabolism[26]. We observed that transcripts encoding genes involved in endocytosis
556 and calcium signaling were enriched among downregulated genes in IRE1$^{\Delta R}$ macrophages (Table
557 S1.2), highlighting the possibility that gene expression regulation by IRE1α may influence
558 phagolysosome fusion. Whether IRE1α has broad roles in phagosome-lysosome fusion, ER-
559 phagosome contact sites, or the degradative capacity of macrophages and other cell types will
560 be an important future direction.

561 IRE1α in the myeloid compartment was shown to drive immunopathology during systemic
562 *C. albicans* infection, and IRE1α ablation in neutrophils prolonged survival of infected hosts in a
563 murine systemic *C. albicans* infection model[14]. In this study, it was revealed that ROS production
564 in *C. albicans* infected neutrophils triggers protein misfolding and IRE1α activation, and
565 subsequent XBP1S production enhanced the production of proinflammatory cytokines, driving
566 fatal kidney immunopathology[14]. Our work complements these findings, uncovering new functions
567 of IRE1α in macrophage antifungal responses during early stages of infection. We similarly found
568 that stimulation of the CLR pathway can trigger IRE1α activation, although we report that protein
569 misfolding is not required for early IRE1α activation in macrophages. Additionally, while IRE1α
570 was not required for neutrophil fungicidal activity, we found that it does support macrophage
571 fungicidal activity. Neutrophils are more effective at killing *C. albicans* than macrophages[87], and
572 presumably utilize distinct fungicidal effectors, although little is known about the mechanisms by
573 which macrophages kill *C. albicans*[43]. A full understanding of the mechanisms by which IRE1α
574 augments macrophage fungicidal activity will require characterization of the effectors of fungal
575 killing in macrophages.

576 In summary, our work suggests that innate immune signaling can trigger non-canonical
577 activation of IRE1α and highlights new roles for IRE1α in the fungicidal capacity of macrophages.
578 These findings will help shape our understanding of the activation and function of IRE1α in

infection and other settings. Protein misfolding-independent activation of IRE1α suggests new paradigms to explore in other contexts, such as sterile inflammation and obesity[83], and a critical role for IRE1α as a sensor of other agents that may perturb cellular homeostasis. Dissection of the molecular mechanisms regulating early IRE1α activation may identify new therapeutic targets for regulation of IRE1α activity. Further, a better understanding of the role of IRE1α in the endocytic pathway will provide fundamental understanding of communication between the ER and endocytic compartments. Overall, these findings reveal exciting roles for a critical component of the UPR during fungal infection with broad potential impacts for our understanding of cell biology.

Supplemental tables

Table S1: RNA-seq data from IRE1 WT and IRE1$^{\Delta R}$ macrophages infected with *C. albicans*.

- **Table S1.1:** Differential gene expression in *C. albicans* infected IRE1$^{\Delta R}$ macrophages compared to IRE1 WT
- **Table S1.2:** Gene ontology analysis of pathways enriched among genes downregulated in *C. albicans* infected IRE1$^{\Delta R}$ macrophages compared to IRE1 WT

Supplemental Movies

Supplemental Movie 1: Live imaging of Fluo4 in *C. albicans*-infected IRE1 WT macrophages

Supplemental Movie 2: Live imaging of Fluo4 in *C. albicans*-infected IRE1$^{\Delta R}$ macrophages

Acknowledgements

We thank the following colleagues who provided cell lines and reagents: Dr. Stacy Horner, Dr. Ling Qi, Dr. Stu Levitz, Dr. Tod Merkel, and Dr. Scott Soleimanpour, as well as Dr. Jonathan Sexton for microscopy equipment and advice, and Dr. Basel Abuaita for immortalization of IRE1$^{fl/fl\ exon20\text{-}21}$ and TLR2/4/9 knockout macrophages and matched controls. We thank members of the O'Meara and O'Riordan labs for discussion. This work was supported by National Institute of Health grants K22 AI137299 (T.R.O.), R01 AI157384 (M.X.D.O.), T32AR007197 (M.J.M.), and T32AI007528 (M.J.M.). Other funding sources include the University of Michigan Pioneer Fellows Program (M.J.M.).

Author contributions

613 Conceptualization: M.J.M., M.X.D.O., and T.R.O. Investigation: M.J.M., M.B.R., B.C.M.,
614 E.B.O., F.M.A., and T.L.S. Formal analysis: M.J.M., T.R.O., M.X.D.O. Software: M.J.M.,
615 M.B.R., B.C.M, E.B.O., and T.R.O. Writing – original draft: M.J.M., T.R.O., and M.X.D.O. Writing
616 – review and editing: M.J.M., M.B.R., B.C.M., E.B.O., F.M.A., T.L.S., M.X.D.O., and T.R.O.
617 Funding acquisition: M.J.M., M.X.D.O., and T.R.O.
618
619 **Competing interests**
620 The authors declare no competing interests.
621
622
623 **Methods**
624
625 **Plasmids.** pLEX-FLAG-Cre-GFP was generated by cloning PCR-amplified N-terminal FLAG
626 tagged Cre-GFP (from pCAG-Cre-GFP; Addgene #13776) (Forward primer:
627 TAAAGCGGCCGCTATGGCCAATTTACTGACCG; Reverse primer:
628 CTCTAGACTCGAGTTAACTTACTTGTACAGCTCGTCCA) coding sequence into the pLEX
629 expression vector using NotI and XhoI restriction sites. pLEX-FLAG-GFP vector was a gift from
630 Dr. Stacy Horner. All plasmids were verified by whole plasmid sequencing (Plasmidsaurus).
631
632 **Cell lines.** All cell lines were incubated at 37ºC with 5% CO_2. Bone marrow-derived macrophages
633 (BMDM) were grown in bone marrow media (BMM), containing modification of Eagle's medium
634 (DMEM; Thermo Fisher Scientific) supplemented with 20% fetal bovine serum (Thermo Fisher
635 Scientific), 30% L929 conditioned media, and 1 mM sodium pyruvate (Thermo Fisher Scientific).
636 BMDM were immortalized (iBMDM) using J2 retrovirus[88]. L-929 cells were cultured in minimum
637 essential Eagle's medium supplemented with 2 mM l-glutamine, 1 mM sodium pyruvate, 1 mM
638 nonessential amino acid, 10 mM HEPES, and 10% FBS. All experiments were performed in
639 experimental media (RPMI supplemented with 3% FBS) unless otherwise indicated. All cell lines
640 were verified as mycoplasma free using the Lookout Mycoplasma PCR Detection Kit (Sigma-
641 Aldrich) and genetic identities were validated by PCR, western blotting, or functional assays.
642 IRE1$^{fl/fl\ exon20\text{-}21}$ (-/+ Cre) mice were a gift from Dr. Ling Qi, CARD9 knockout mice and littermate
643 WT mice were a gift from Dr. Stu Levitz, TLR2/4/9 knockout mice and littermate WT mice were a
644 gift from Dr. Tod Merkel, and TRAF6$^{fl/fl}$ mice were a gift from Dr. Scott Soleimanpour. To generate
645 IRE1$^{\Delta R}$ and control IRE1 WT macrophages, iBMDM from IRE1$^{fl/fl\ exon20\text{-}21}$ mice with and without
646 inducible Cre expression were treated with 4-hydroxy tamoxifen for 24 hours, followed by clonal

647 expansion of cell lines. IRE1$^{\Delta R}$ macrophages were confirmed by immunoblotting and *Xbp1*
648 splicing assays. To generate TRAF6 KO cell lines, first lentiviral particles encoding GFP or CRE-
649 GFP were generated by harvesting supernatant 72 h post-transfection of 293T cells with pLEX-
650 FLAG-GFP, or pLEX-FLAG-Cre-GFP, and the packaging plasmids psPAX2 and pMD2.G
651 (provided by Dr. Stacy Horner). These supernatants were then used to transduce TRAF6$^{fl/fl}$
652 iBMDM for 24 hours. Following transduction, cells were selected in 3 µg/mL puromycin (Sigma)
653 for 48 hours and single cell colonies were isolated. TRAF6 deletion in CRE-GFP cell lines was
654 verified by immunoblotting in CRE-GFP expressing TRAF6$^{fl/fl}$ iBMDM clonal cell lines (KO-1 and
655 KO-2). GFP-expressing TRAF6$^{fl/fl}$ iBMDM clonal cell lines were used as a control (WT-1 and WT-
656 2).
657
658 ***Candida albicans* infection and LPS treatment.** *C. albicans* cells were cultured at 30 °C in YPD
659 liquid media (1% yeast extract, 2% peptone, 2% dextrose) with constant agitation. All strains were
660 maintained as frozen stocks of 25% glycerol at -80 °C. For infection of iBMDM, macrophages
661 were seeded in experimental plates overnight at approximately 80% confluence. Experimental
662 media (RPMI (Gibco), supplemented with 3% FBS) was inoculated with log-phase *C. albicans*
663 cells counted for a calculated MOI of 1. LPS from *E. coli* O111:B4 (Sigma-Aldrich L2630) was
664 diluted to 100 ng/mL in experimental media for all experiments.
665
666 **RT-qPCR.** Total cellular RNA was extracted from all samples using TRIzol (Thermo Fisher
667 Scientific), according to manufacturer's protocol. RNA was then reverse transcribed using the
668 iScript cDNA synthesis kit (Bio-Rad) as per the manufacturer's instructions. The resulting cDNA
669 was diluted 1:5 in nuclease-free H_2O. RT-qPCR was performed in triplicate using the PowerUP
670 SYBR Green PCR master mix (Thermo Fisher Scientific) and the Bio-Rad CFX Opus 384 Real-
671 Time RT-PCR systems. *Xbp1-S* transcript was amplified using primers Forward:
672 GCTGAGTCCGCAGCAGGT and Reverse: CAGGGTCCAACTTGTCCAGAAT. *Gapdh* transcript
673 was amplified using primers Forward: CATCACTGCCACCCAGAAGACTG and Reverse:
674 ATGCCAGTGAGCTTCCCGTTCAG.
675
676 **Semi-quantitative *Xbp1* splicing gel analysis.** Total cellular RNA was extracted using TRIzol
677 (Thermo Fisher Scientific), according to the manufacturer's protocol. RNA was then reverse
678 transcribed using the iScript cDNA synthesis kit (Bio-Rad) as per the manufacturer's instructions.
679 The resulting cDNA was diluted 1:5 in nuclease-free H2O. *Xbp1* transcript was amplified by PCR
680 using primers XF and XR, followed by PCR cleanup using the Qiagen PCR Cleanup Kit. The

681 amplified *Xbp1* product was then digested using PstI, which recognizes a cleavage site within the
682 26 base pair intron that is removed by IRE1α activity[89]. Following digestion, *Xbp1* bands were
683 resolved on a 2% agarose gel and visualized by ethidium bromide staining and imaging on a
684 BioRad gel dock.
685
686 **Immunoblotting.** Cells were lysed in a modified radioimmunoprecipitation assay (RIPA) buffer
687 (10 mM Tris [pH 7.5], 150 mM NaCl, 0.5% sodium deoxycholate, and 1% Triton X-100)
688 supplemented with protease and phosphatase inhibitor cocktail (Millipore-Sigma) and clarified
689 lysates were harvested by centrifugation. Quantified protein (between 5 and 15 mg) was added
690 to a 4X SDS protein sample buffer (40% glycerol, 240 mM Tris-HCl [pH 6.8], 8% SDS, 0.04%
691 bromophenol blue, 5% beta-mercaptoethanol), resolved by SDS/PAGE, and transferred to
692 nitrocellulose membranes in a 25 mM Tris-192 mM glycine-0.01% SDS buffer. Membranes were
693 stained with Revert 700 total protein stain (LI-COR Biosciences), then blocked in 3% bovine
694 serum albumin. Membranes were incubated with primary antibodies for 2 hours at room
695 temperature or overnight at 4C. After washing with PBS-T buffer (1 3 PBS, 0.05% Tween 20),
696 membranes were incubated with species-specific IRDye-conjugated antibodies (Licor, 1:5000) for
697 1 hour at room temperature, followed by imaging on an Odyssey imaging system (LI-COR
698 Biosciences). The following antibodies were used for immunoblotting: rabbit anti-IRE1α
699 (CellSignaling 3924, 1:1000); rabbit anti-XBP1 (Abcam AB-37152, 1:1000); mouse anti-ACTIN
700 (ThermoFisher ACTN05 (C4), 1:5000); rabbit anti-TRAF6 (Abcam ab40675, 1:1000); rabbit anti-
701 CARD9 (CellSignaling 12283, 1:1000).
702
703 **Quantification of immunoblots.** Following imaging using the LI-COR Odyssey imager,
704 immunoblots were quantified using ImageStudio Lite software, and raw values were normalized
705 to total protein (Revert 700 total protein stain) or ACTIN for each condition.
706
707 **Thioflavin T assay.** iBMDM ($2*10^5$ cells/well) were seeded in a 24-well plate overnight and then
708 infected with *C. albicans*, or treated with LPS or thapsigargin for indicated timepoints. Thioflavin
709 T (Cayman Chemical, 5 μM) was added 2 hours prior to endpoint. Cells were scraped into ice
710 cold PBS and thioflavin T intensity was measured on a BD LSRFortessa X-20 flow cytometer.

711 **RNA-sequencing.** iBMDM were seeded in 6-well plates overnight (10^6 cells/well) then infected
712 with *C. albicans* (MOI 1) or mock treated (4 h), then harvested in TRIzol reagent (Thermo Fisher)
713 and RNA extraction was performed according to manufacturer protocol. Samples were then

714 treated with Turbo DNase I (Thermo Fisher) according to manufacturer protocol and incubated at
715 37 ˚C for 30 min, followed by phenol/chloroform extraction and ethanol precipitation overnight.
716 RNA concentrations were then normalized. PolyA enrichment was performed and sequencing
717 libraries were prepared and sequenced on an Illumina NovaSeq 6000 with 150 bp paired-end
718 reads by Novogene.

719 **RNA-seq analysis.** RNA-seq analysis was performed in Galaxy (usegalaxy.org). Reads were
720 evaluated using FastQC and trimmed using cutadapt[90], followed by quantification of transcripts
721 from the GRCm38 mouse genome using Kallisto[91]. Differential gene expression between IRE1$^{\Delta R}$
722 and IRE1 WT macrophages following *C. albicans* infection (Table S1.1) was compared using
723 DESeq2[92]. Gene ontology analysis was performed on significantly upregulated or downregulated
724 genes in each data set using g:Profiler[93].

725

726 **ELISA.** iBMDM ($3*10^4$ cells/well) were seeded in 96-well plates overnight, then primed with LPS
727 (100 ng/mL) for 3 hours prior to *C. albicans* infection (MOI 1). Supernatants were collected at 5
728 hpi and submitted to the University of Michigan Cancer Center Immunology Core for quantification
729 of secreted IL-1β, TNF, and IL-6.

730

731 **Quantification of phagocytosis of *C. albicans*.** iBMDM ($3*10^4$ cells/well) were seeded in a 96-
732 well plastic-bottom imaging plate (PerkinElmer) overnight and then infected with *C. albicans* (MOI
733 1) for 30 minutes. Wells were then fixed in 4% parafolmaldehyde (Electron Microscopy Sciences)
734 for 15 minutes, washed with PBS (ThermoFisher), and blocked with PBS containing 3% bovine
735 serum albumin (ThermoFisher) and 5% normal goat serum (Invitrogen) for 30 minutes. FITC-
736 conjugated anti-*Candida* antibody (LSBio LS-C103355, 1:2000) was diluted in blocking buffer and
737 added for 1 hour with agitation to label extracellular *C. albicans*, followed by 3 5 minute washes
738 with PBS. Wells were then permeabilized in 0.1% Triton-X 100 (Sigma-Aldrich) for 15 minutes,
739 followed by 3 washes in PBS. Calcofluor white (Sigma-Aldrich, 1:100) was diluted in blocking
740 buffer and added to wells for 30 minutes with agitation, followed by 3 5 minute PBS washes, and
741 images were captured on a BioTek Lionheart FX automated microscope. A CellProfiler pipeline
742 was developed to segment extracellular (FITC+) and total (FITC+ CFW+) *C. albicans*, and the
743 percent phagocytosed by macrophages was calculated as 100 * (1 – (FITC+ / FITC+ CFW+)).

744

745 **Quantification of phagolysosomal fusion.** iBMDM ($3*10^4$ cells/well) were seeded in a 96-well
746 plastic-bottom imaging plate (PerkinElmer) overnight and then infected with *C. albicans* SC5314

747 cells expressing near-infrared fluorescent protein (iRFP) driven by the *pENO1* promoter[94] (MOI
748 1) at indicated timepoints. Wells were then fixed in 4% paraformaldehyde (Electron Microscopy
749 Sciences) for 15 minutes, washed with PBS (ThermoFisher), and permeabilized in 0.1% Triton-X
750 100 (Sigma-Aldrich) for 15 minutes, followed by 3 washes in PBS. Wells were blocked with PBS
751 containing 0.01% Triton-X 100, 3% bovine serum albumin (ThermoFisher) and 5% normal goat
752 serum (Invitrogen) for 30 minutes. Primary antibodies rat anti-LAMP1 (DSHB 1D4B, 1:50) and
753 rabbit anti-LC3 (MBL pM036, 1:400) were diluted in block buffer and added to wells for 1 hour,
754 followed by 3 5 minute washes with PBS. Alexafluor-conjugated secondary antibodies goat anti-
755 rat 594 and goat anti-rabbit 488 were diluted 1:500 in blocking buffer with DAPI (1:1000) and
756 added to wells for 1 hour, followed by 3 5 minute PBS washes, and images were captured on a
757 Yokogawa CellVoyager CQ1 automated confocal microscope. A CellProfiler pipeline was
758 developed to segment *C. albicans* and measure the mean intensity of LAMP1 enriched at the *C.*
759 *albicans* network.
760
761 **Calcium flux assay and analysis.** iBMDM ($3*10^4$ cells/well) were seeded in a 96-well plastic-
762 bottom imaging plate (PerkinElmer) overnight and then loaded with Fluo-4 (1:1000; Fluo-4
763 Calcium Imaging Kit; Invitrogen) and CellTracker Red (1:2000; Invitrogen) according to
764 manufacturer protocol for 20 minutes at 37ºC, then 20 minutes at room temperature. Staining
765 media was then removed, followed by a wash with room-temperature media. Cells were infected
766 with *C. albicans* SC5314 cells expressing near-infrared fluorescent protein (iRFP) driven by the
767 *pENO1* promoter[94] (MOI 2), immediately followed by live imaging captured on a Yokogawa
768 CellVoyager CQ1 automated confocal microscope with incubation at 37ºC with 5% CO_2. Images
769 were captured every 90 seconds for 1 hour.
770 Analysis of initial Fluo-4 intensity was performed on time 0 images using a CellProfiler pipeline to
771 identify cells and measure the mean fluorescence intensity of Fluo-4. For analysis of cellular
772 calcium flux, the Python package spacr (https://github.com/EinarOlafsson/spacr) was used to
773 segment and track cells over time and quantify single cell calcium oscillations. Cells were
774 delineated with the Cellpose cyto model[95] from CellTracker Red staining. Centroids of identified
775 cell objects were tracked using the Trackpy particle-tracking algorithm[96]. Fluo-4 mean intensity
776 values were normalized between 0 and 1 and corrected for photobleaching across the time series
777 using an exponential decay model to enable the detection of calcium spikes above a threshold of
778 0.25 with the find_peaks function from scipy[97]. Peaks were then enumerated and characterized
779 by collecting peak frequency and amplitude for each condition.

780 Analysis of phagosomal calcium influx was performed at 20 minutes post-infection using NIH
781 Fiji/ImageJ. The line tool was used to calculate the mean fluorescence intensity of Fluo4 rings
782 within *C. albicans*-containing phagosomes, which were measured relative to the mean
783 fluorescence intensity of the whole parental macrophage. Calcium-high phagosomes were
784 defined as phagosomes with Fluo-4 intensity >1.25-fold higher than the mean fluorescence
785 intensity of the parent macrophage.
786
787 **Macrophage fungicidal activity assay.** iBMDM ($3*10^4$ cells/well) were seeded in a 96-well
788 plastic-bottom imaging plate (PerkinElmer) overnight. Approximately 10^7 *C. albicans* SC5314
789 cells expressing iRFP from an overnight culture were stained with calcofluor white (CFW; 100
790 µg/mL) for 10 minutes in the dark. Cells were then washed twice with PBS prior to macrophage
791 infection at MOI = 1. Images of infected cultures were captured every 20 minutes on a BioTek
792 Lionheart FX automated microscope with incubation at 37C and 5% CO2. Fungal killing was
793 quantified at 7 hours post-infection by calculating killed *C. albicans* ($iRFP^-$ CFW^+) over total *C.*
794 *albicans* ($iRFP^{-/+}$ CFW^+), with at least 200 *C. albicans* cells counted per condition.
795
796 **LysoSensor.** iBMDM ($2*10^5$ cells/well) were seeded in a 24-well plate overnight and then infected
797 with *C. albicans* for 2 hours prior to addition of LysoSensor Yellow/Blue DND-160 (Thermo Fisher,
798 500 nM) for 2 minutes in experimental media. Wells were then washed 3 times in ice-cold PBS
799 and scraped for plate reader analysis. Suspended cells were added to a black-bottom 96-well
800 plate and absorbance and emission were measured at 329 nm Abs, 440 nm Em and 384 nm Abs,
801 540 nm Em to measure fluorescence intensity in high and low pH environments, respectively. The
802 intensity of the low pH measurement was divided by the intensity of the high pH measurement,
803 and these results were normalized to IRE1 WT Mock to determine the relative acidity of each
804 condition.
805
806 **Sulforhodamine B Assay and *C. albicans* hyphal length measurement.** iBMDM ($3*10^4$
807 cells/well) were seeded in a 96-well plastic-bottom imaging plate (PerkinElmer) overnight, then
808 sulforhodamine B (SRB) (Sigma-Aldrich, 150 µg/mL) was added to wells for 1 hour. SRB was
809 then washed out and wells were with *C. albicans* expressing iRFP (MOI 1) and live imaging was
810 performed on a Yokogawa CellVoyager CQ1 automated confocal microscope every 30 minutes
811 for 5 hours. A CellProfiler pipeline was developed to segment *C. albicans* and measure the total
812 area covered by hyphae, and the mean intensity of SRB enriched at the *C. albicans* network was
813 measured at each timepoint.

814

815 ***In vivo* systemic *C. albicans* challenge experiments.** Overnight cultures of *C. albicans*
816 expressing iRFP were sub-cultured at a starting OD600 of 0.1 and grown for 4 hours, then pelleted
817 by centrifugation and resuspended in PBS for delivery to the bloodstream of mice. 8-12 week old
818 male and female mice lacking IRE1α activity in macrophages and neutrophils ($IRE1^{fl/fl}$ $LysM^{Cre}$)
819 and littermate controls ($IRE1^{fl/fl}$) were systemically infected with iRFP-expressing *C. albicans* (10^6
820 CFU) by retro-orbital injection. At 24 hours post-infection, mice were euthanized and serum was
821 collected by cardiac puncture, followed by isolation of serum using centrifugation of serum
822 collection tubes. Serum samples were submitted to the University of Michigan Cancer Center
823 Immunology Core for quantification of secreted IL-1β, IL-1Ra, TNF, and IL-6 by ELISA. Kidneys
824 were isolated and dissociated by mechanical separation through a 70 µm cell strainer, followed
825 by red blood cell lysis (eBioscience 10X RBC Lysis Buffer). To quantify *C. albicans* viability in
826 kidney samples, $2*10^6$ cells per sample were subjected to immunofluorescence staining. Total *C.*
827 *albicans* was stained using a FITC-conjugated anti-*Candida* antibody (1:1000; Meridian
828 Bioscience), and myeloid cells were stained with Brilliant Violet 421-conjugated anti-CD11b
829 antibody (1:100; Biolegend) for 1 hour in the dark with gentle agitation. After immunostaining,
830 samples were plated in 96-well plastic-bottom imaging plates (PerkinElmer) coated with poly-D-
831 Lysine (Gibco) and imaging was performed on a Yokogawa CellVoyager CQ1 automated confocal
832 microscope. A CellProfiler pipeline was developed to segment *C. albicans* and host myeloid cells.
833 Total *C. albicans* were identified from kidney tissue and myeloid cells using FITC signal, and
834 viability was measured using iRFP intensity.

835

836

837 **Lead Contact and Materials Availability**. Further information and requests for resources and
838 reagents should be directed to and will be fulfilled by the Lead Contacts, Teresa O'Meara
839 (tromeara@umich.edu) and/or Mary O'Riordan (oriordan@umich.edu)

840

841 **Data Availability.** All raw data related to RNA-seq are available through GEO (accession number:
842 GSE244303). All raw data related to microscopy are available upon request.

843

844 **Code Availability.** CellProfiler pipelines for image quantification are available as Supplementary
845 Materials (files S2-S5). Software for cellular calcium flux analysis are available from GitHub
846 (https://github.com/EinarOlafsson/spacr).

847

848 **References**

849

850 1. Muralidharan, S., and Mandrekar, P. (2013). Cellular stress response and innate immune
851 signaling: integrating pathways in host defense and inflammation. J. Leukoc. Biol. *94*, 1167–
852 1184.
853 2. Chovatiya, R., and Medzhitov, R. (2014). Stress, inflammation, and defense of homeostasis.
854 Mol. Cell *54*, 281–288.
855 3. Grootjans, J., Kaser, A., Kaufman, R.J., and Blumberg, R.S. (2016). The unfolded protein
856 response in immunity and inflammation. Nat. Rev. Immunol. *16*, 469–484.
857 4. Choi, J.-A., and Song, C.-H. (2019). Insights Into the Role of Endoplasmic Reticulum Stress
858 in Infectious Diseases. Front. Immunol. *10*, 3147.
859 5. Read, A., and Schröder, M. (2021). The Unfolded Protein Response: An Overview. Biology
860 *10*. 10.3390/biology10050384.
861 6. Martinon, F., Chen, X., Lee, A.-H., and Glimcher, L.H. (2010). TLR activation of the
862 transcription factor XBP1 regulates innate immune responses in macrophages. Nat.
863 Immunol. *11*, 411–418.
864 7. Saito, A., and Imaizumi, K. (2018). Unfolded Protein Response-Dependent Communication
865 and Contact among Endoplasmic Reticulum, Mitochondria, and Plasma Membrane. Int. J.
866 Mol. Sci. *19*. 10.3390/ijms19103215.
867 8. Watowich, S.S., Morimoto, R.I., and Lamb, R.A. (1991). Flux of the paramyxovirus
868 hemagglutinin-neuraminidase glycoprotein through the endoplasmic reticulum activates
869 transcription of the GRP78-BiP gene. J. Virol. *65*, 3590–3597.
870 9. Tardif, K.D., Mori, K., Kaufman, R.J., and Siddiqui, A. (2004). Hepatitis C virus suppresses
871 the IRE1-XBP1 pathway of the unfolded protein response. J. Biol. Chem. *279*, 17158–17164.
872 10. Bronner, D.N., Abuaita, B.H., Chen, X., Fitzgerald, K.A., Nuñez, G., He, Y., Yin, X.-M., and
873 O'Riordan, M.X.D. (2015). Endoplasmic Reticulum Stress Activates the Inflammasome via
874 NLRP3- and Caspase-2-Driven Mitochondrial Damage. Immunity *43*, 451–462.
875 11. Baruch, M., Hertzog, B.B., Ravins, M., Anand, A., Cheng, C.Y., Biswas, D., Tirosh, B., and
876 Hanski, E. (2014). Induction of endoplasmic reticulum stress and unfolded protein response
877 constitutes a pathogenic strategy of group A streptococcus. Front. Cell. Infect. Microbiol. *4*,
878 105.
879 12. Abuaita, B.H., Burkholder, K.M., Boles, B.R., and O'Riordan, M.X. (2015). The Endoplasmic
880 Reticulum Stress Sensor Inositol-Requiring Enzyme 1α Augments Bacterial Killing through
881 Sustained Oxidant Production. MBio *6*, e00705.
882 13. Abuaita, B.H., Schultz, T.L., and O'Riordan, M.X. (2018). Mitochondria-Derived Vesicles
883 Deliver Antimicrobial Reactive Oxygen Species to Control Phagosome-Localized
884 Staphylococcus aureus. Cell Host Microbe *24*, 625-636.e5.
885 14. Awasthi, D., Chopra, S., Cho, B.A., Emmanuelli, A., Sandoval, T.A., Hwang, S.-M., Chae,
886 C.-S., Salvagno, C., Tan, C., Vasquez-Urbina, L., et al. (2023). Inflammatory ER stress
887 responses dictate the immunopathogenic progression of systemic candidiasis. J. Clin.
888 Invest. 10.1172/JCI167359.
889 15. Celli, J., and Tsolis, R.M. (2015). Bacteria, the endoplasmic reticulum and the unfolded
890 protein response: friends or foes? Nat. Rev. Microbiol. *13*, 71–82.
891 16. Belyy, V., Zuazo-Gaztelu, I., Alamban, A., Ashkenazi, A., and Walter, P. (2022). Endoplasmic
892 reticulum stress activates human IRE1α through reversible assembly of inactive dimers into
893 small oligomers. Elife *11*. 10.7554/eLife.74342.
894 17. Yoshida, H., Matsui, T., Yamamoto, A., Okada, T., and Mori, K. (2001). XBP1 mRNA is
895 induced by ATF6 and spliced by IRE1 in response to ER stress to produce a highly active
896 transcription factor. Cell *107*, 881–891.

897 18. Cox, J.S., and Walter, P. (1996). A novel mechanism for regulating activity of a transcription
898 factor that controls the unfolded protein response. Cell *87*, 391–404.
899 19. Kaufman, R.J. (1999). Stress signaling from the lumen of the endoplasmic reticulum:
900 coordination of gene transcriptional and translational controls. Genes Dev. *13*, 1211–1233.
901 20. Park, S.-M., Kang, T.-I., and So, J.-S. (2021). Roles of XBP1s in Transcriptional Regulation
902 of Target Genes. Biomedicines *9*. 10.3390/biomedicines9070791.
903 21. Qiu, Q., Zheng, Z., Chang, L., Zhao, Y.-S., Tan, C., Dandekar, A., Zhang, Z., Lin, Z., Gui,
904 M., Li, X., et al. (2013). Toll-like receptor-mediated IRE1α activation as a therapeutic target
905 for inflammatory arthritis. EMBO J. *32*, 2477–2490.
906 22. Nguyen, L.C., Renner, D.M., Silva, D., Yang, D., Parenti, N., Medina, K.M., Nicolaescu, V.,
907 Gula, H., Drayman, N., Valdespino, A., et al. (2022). SARS-CoV-2 diverges from other
908 betacoronaviruses in only partially activating the IRE1α/XBP1 ER stress pathway in human
909 lung-derived cells. bioRxiv. 10.1101/2021.12.30.474519.
910 23. Carreras-Sureda, A., Zhang, X., Laubry, L., Brunetti, J., Koenig, S., Wang, X., Castelbou, C.,
911 Hetz, C., Liu, Y., Frieden, M., et al. (2023). The ER stress sensor IRE1 interacts with STIM1
912 to promote store-operated calcium entry, T cell activation, and muscular differentiation. Cell
913 Rep. *42*, 113540.
914 24. English, B.C., Savage, H.P., Mahan, S.P., Diaz-Ochoa, V.E., Young, B.M., Abuaita, B.H.,
915 Sule, G., Knight, J.S., O'Riordan, M.X., Bäumler, A.J., et al. (2023). The IRE1α-XBP1
916 Signaling Axis Promotes Glycolytic Reprogramming in Response to Inflammatory Stimuli.
917 MBio *14*, e0306822.
918 25. Yu, C.-Y., Hsu, Y.-W., Liao, C.-L., and Lin, Y.-L. (2006). Flavivirus infection activates the
919 XBP1 pathway of the unfolded protein response to cope with endoplasmic reticulum stress.
920 J. Virol. *80*, 11868–11880.
921 26. Carreras-Sureda, A., Jaña, F., Urra, H., Durand, S., Mortenson, D.E., Sagredo, A., Bustos,
922 G., Hazari, Y., Ramos-Fernández, E., Sassano, M.L., et al. (2019). Non-canonical function
923 of IRE1α determines mitochondria-associated endoplasmic reticulum composition to control
924 calcium transfer and bioenergetics. Nat. Cell Biol. *21*, 755–767.
925 27. Iovino, M., Colonval, M., Wilkin, C., L'homme, L., Lassence, C., Campas, M., Peulen, O., de
926 Tullio, P., Piette, J., and Legrand-Poels, S. (2023). Novel XBP1s-independent function of
927 IRE1 RNase in HIF-1α-mediated glycolysis upregulation in human macrophages upon
928 stimulation with LPS or saturated fatty acid. Front. Immunol. *14*, 1204126.
929 28. Anderson, F.M., Visser, N.D., Amses, K.R., Hodgins-Davis, A., Weber, A.M., Metzner, K.M.,
930 McFadden, M.J., Mills, R.E., O'Meara, M.J., James, T.Y., et al. (2023). Candida albicans
931 selection for human commensalism results in substantial within-host diversity without
932 decreasing fitness for invasive disease. PLoS Biol. *21*, e3001822.
933 29. Lionakis, M.S., Swamydas, M., Fischer, B.G., Plantinga, T.S., Johnson, M.D., Jaeger, M.,
934 Green, N.M., Masedunskas, A., Weigert, R., Mikelis, C., et al. (2013). CX3CR1-dependent
935 renal macrophage survival promotes Candida control and host survival. J. Clin. Invest. *123*,
936 5035–5051.
937 30. Martino, P., Girmenia, C., Venditti, M., Micozzi, A., Santilli, S., Burgio, V.L., and Mandelli, F.
938 (1989). Candida colonization and systemic infection in neutropenic patients. A retrospective
939 study. Cancer *64*, 2030–2034.
940 31. Netea, M.G., Brown, G.D., Kullberg, B.J., and Gow, N.A.R. (2008). An integrated model of
941 the recognition of Candida albicans by the innate immune system. Nat. Rev. Microbiol. *6*,
942 67–78.
943 32. McKenzie, C.G.J., Koser, U., Lewis, L.E., Bain, J.M., Mora-Montes, H.M., Barker, R.N., Gow,
944 N.A.R., and Erwig, L.P. (2010). Contribution of Candida albicans cell wall components to
945 recognition by and escape from murine macrophages. Infect. Immun. *78*, 1650–1658.

946 33. Qian, Q., Jutila, M.A., Van Rooijen, N., and Cutler, J.E. (1994). Elimination of mouse splenic
947 macrophages correlates with increased susceptibility to experimental disseminated
948 candidiasis. J. Immunol. *152*, 5000–5008.
949 34. van de Veerdonk, F.L., Gresnigt, M.S., Oosting, M., van der Meer, J.W.M., Joosten, L.A.B.,
950 Netea, M.G., and Dinarello, C.A. (2014). Protective host defense against disseminated
951 candidiasis is impaired in mice expressing human interleukin-37. Front. Microbiol. *5*, 762.
952 35. Netea, M.G., Joosten, L.A.B., van der Meer, J.W.M., Kullberg, B.-J., and van de Veerdonk,
953 F.L. (2015). Immune defence against Candida fungal infections. Nat. Rev. Immunol. *15*, 630–
954 642.
955 36. Hise, A.G., Tomalka, J., Ganesan, S., Patel, K., Hall, B.A., Brown, G.D., and Fitzgerald, K.A.
956 (2009). An essential role for the NLRP3 inflammasome in host defense against the human
957 fungal pathogen Candida albicans. Cell Host Microbe *5*, 487–497.
958 37. Joly, S., Ma, N., Sadler, J.J., Soll, D.R., Cassel, S.L., and Sutterwala, F.S. (2009). Cutting
959 edge: Candida albicans hyphae formation triggers activation of the Nlrp3 inflammasome. J.
960 Immunol. *183*, 3578–3581.
961 38. Gross, O., Poeck, H., Bscheider, M., Dostert, C., Hannesschläger, N., Endres, S., Hartmann,
962 G., Tardivel, A., Schweighoffer, E., Tybulewicz, V., et al. (2009). Syk kinase signalling
963 couples to the Nlrp3 inflammasome for anti-fungal host defence. Nature *459*, 433–436.
964 39. Wellington, M., Koselny, K., and Krysan, D.J. (2012). Candida albicans morphogenesis is
965 not required for macrophage interleukin 1β production. MBio *4*, e00433-12.
966 40. Wellington, M., Koselny, K., Sutterwala, F.S., and Krysan, D.J. (2014). Candida albicans
967 triggers NLRP3-mediated pyroptosis in macrophages. Eukaryot. Cell *13*, 329–340.
968 41. O'Meara, T.R., Veri, A.O., Ketela, T., Jiang, B., Roemer, T., and Cowen, L.E. (2015). Global
969 analysis of fungal morphology exposes mechanisms of host cell escape. Nat. Commun. *6*,
970 6741.
971 42. Diamond, R.D., Lyman, C.A., and Wysong, D.R. (1991). Disparate effects of interferon-
972 gamma and tumor necrosis factor-alpha on early neutrophil respiratory burst and fungicidal
973 responses to Candida albicans hyphae in vitro. J. Clin. Invest. *87*, 711–720.
974 43. Newman, S.L., Bhugra, B., Holly, A., and Morris, R.E. (2005). Enhanced killing of Candida
975 albicans by human macrophages adherent to type 1 collagen matrices via induction of
976 phagolysosomal fusion. Infect. Immun. *73*, 770–777.
977 44. Westman, J., Walpole, G.F.W., Kasper, L., Xue, B.Y., Elshafee, O., Hube, B., and Grinstein,
978 S. (2020). Lysosome Fusion Maintains Phagosome Integrity during Fungal Infection. Cell
979 Host Microbe *28*, 798-812.e6.
980 45. Seegren, P.V., Downs, T.K., Stremska, M.E., Harper, L.R., Cao, R., Olson, R.J., Upchurch,
981 C.M., Doyle, C.A., Kennedy, J., Stipes, E.L., et al. (2020). Mitochondrial Ca2 Signaling Is an
982 Electrometabolic Switch to Fuel Phagosome Killing. Preprint, 10.1016/j.celrep.2020.108411
983 10.1016/j.celrep.2020.108411.
984 46. Vesely, E.M., Williams, R.B., Konopka, J.B., and Lorenz, M.C. (2017). N-Acetylglucosamine
985 Metabolism Promotes Survival of Candida albicans in the Phagosome. mSphere *2*.
986 10.1128/mSphere.00357-17.
987 47. Iwawaki, T., Akai, R., Yamanaka, S., and Kohno, K. (2009). Function of IRE1 alpha in the
988 placenta is essential for placental development and embryonic viability. Proc. Natl. Acad.
989 Sci. U. S. A. *106*, 16657–16662.
990 48. Glazier, V.E., Kramara, J., Ollinger, T., Solis, N.V., Zarnowski, R., Wakade, R.S., Kim, M.-
991 J., Weigel, G.J., Liang, S.-H., Bennett, R.J., et al. (2023). The Candida albicans reference
992 strain SC5314 contains a rare, dominant allele of the transcription factor Rob1 that
993 modulates filamentation, biofilm formation, and oral commensalism. MBio, e0152123.
994 49. Hardison, S.E., and Brown, G.D. (2012). C-type lectin receptors orchestrate antifungal
995 immunity. Nat. Immunol. *13*, 817–822.

50. Poltorak, A., Smirnova, I., He, X., Liu, M.Y., Van Huffel, C., McNally, O., Birdwell, D., Alejos, E., Silva, M., Du, X., et al. (1998). Genetic and physical mapping of the Lps locus: identification of the toll-4 receptor as a candidate gene in the critical region. Blood Cells Mol. Dis. *24*, 340–355.
51. Hsu, Y.-M.S., Zhang, Y., You, Y., Wang, D., Li, H., Duramad, O., Qin, X.-F., Dong, C., and Lin, X. (2007). The adaptor protein CARD9 is required for innate immune responses to intracellular pathogens. Nat. Immunol. *8*, 198–205.
52. Netea, M.G., Van Der Graaf, C.A.A., Vonk, A.G., Verschueren, I., Van Der Meer, J.W.M., and Kullberg, B.J. (2002). The role of toll-like receptor (TLR) 2 and TLR4 in the host defense against disseminated candidiasis. J. Infect. Dis. *185*, 1483–1489.
53. Kawai, T., and Akira, S. (2010). The role of pattern-recognition receptors in innate immunity: update on Toll-like receptors. Nat. Immunol. *11*, 373–384.
54. Gorjestani, S., Darnay, B.G., and Lin, X. (2012). Tumor necrosis factor receptor-associated factor 6 (TRAF6) and TGFβ-activated kinase 1 (TAK1) play essential roles in the C-type lectin receptor signaling in response to Candida albicans infection. J. Biol. Chem. *287*, 44143–44150.
55. Beriault, D.R., and Werstuck, G.H. (2013). Detection and quantification of endoplasmic reticulum stress in living cells using the fluorescent compound, Thioflavin T. Biochim. Biophys. Acta *1833*, 2293–2301.
56. Ghavami, M., and Fairn, G.D. (2022). Endoplasmic reticulum-Phagosome contact sites from the cradle to the grave. Front Cell Dev Biol *10*, 1074443.
57. Vylkova, S., and Lorenz, M.C. (2014). Modulation of phagosomal pH by Candida albicans promotes hyphal morphogenesis and requires Stp2p, a regulator of amino acid transport. PLoS Pathog. *10*, e1003995.
58. Danhof, H.A., and Lorenz, M.C. (2015). The Candida albicans ATO Gene Family Promotes Neutralization of the Macrophage Phagolysosome. Infect. Immun. *83*, 4416–4426.
59. Boron, W.F., and De Weer, P. (1976). Intracellular pH transients in squid giant axons caused by CO2, NH3, and metabolic inhibitors. J. Gen. Physiol. *67*, 91–112.
60. Hollien, J., and Weissman, J.S. (2006). Decay of endoplasmic reticulum-localized mRNAs during the unfolded protein response. Science *313*, 104–107.
61. Hollien, J., Lin, J.H., Li, H., Stevens, N., Walter, P., and Weissman, J.S. (2009). Regulated Ire1-dependent decay of messenger RNAs in mammalian cells. J. Cell Biol. *186*, 323–331.
62. Upton, J.-P., Wang, L., Han, D., Wang, E.S., Huskey, N.E., Lim, L., Truitt, M., McManus, M.T., Ruggero, D., Goga, A., et al. (2012). IRE1α cleaves select microRNAs during ER stress to derepress translation of proapoptotic Caspase-2. Science *338*, 818–822.
63. Acosta-Alvear, D., Karagöz, G.E., Fröhlich, F., Li, H., Walther, T.C., and Walter, P. (2018). The unfolded protein response and endoplasmic reticulum protein targeting machineries converge on the stress sensor IRE1. Elife *7*. 10.7554/eLife.43036.
64. Mencacci, N.E., Rubio-Agusti, I., Zdebik, A., Asmus, F., Ludtmann, M.H.R., Ryten, M., Plagnol, V., Hauser, A.-K., Bandres-Ciga, S., Bettencourt, C., et al. (2015). A missense mutation in KCTD17 causes autosomal dominant myoclonus-dystonia. Am. J. Hum. Genet. *96*, 938–947.
65. Burk, S.E., Lytton, J., MacLennan, D.H., and Shull, G.E. (1989). cDNA cloning, functional expression, and mRNA tissue distribution of a third organellar Ca2+ pump. J. Biol. Chem. *264*, 18561–18568.
66. Besprozvannaya, M., Dickson, E., Li, H., Ginburg, K.S., Bers, D.M., Auwerx, J., and Nunnari, J. (2018). GRAM domain proteins specialize functionally distinct ER-PM contact sites in human cells. Elife *7*. 10.7554/eLife.31019.
67. Wu, Y., Huang, P., and Dong, X.-P. (2021). Lysosomal Calcium Channels in Autophagy and Cancer. Cancers *13*. 10.3390/cancers13061299.

1046 68. Westman, J., Grinstein, S., and Maxson, M.E. (2019). Revisiting the role of calcium in
1047 phagosome formation and maturation. J. Leukoc. Biol. *106*, 837–851.
1048 69. O'Meara, T.R., Duah, K., Guo, C.X., Maxson, M.E., Gaudet, R.G., Koselny, K., Wellington,
1049 M., Powers, M.E., MacAlpine, J., O'Meara, M.J., et al. (2018). High-Throughput Screening
1050 Identifies Genes Required for Candida albicans Induction of Macrophage Pyroptosis. MBio
1051 *9*. 10.1128/mBio.01581-18.
1052 70. Yang, M., Walpole, G.F.W., and Westman, J. (2020). Maintaining phagosome integrity
1053 during fungal infection: do or die? Microb. Cell Fact. *7*, 323–325.
1054 71. Uwamahoro, N., Verma-Gaur, J., Shen, H.-H., Qu, Y., Lewis, R., Lu, J., Bambery, K.,
1055 Masters, S.L., Vince, J.E., Naderer, T., et al. (2014). The pathogen Candida albicans hijacks
1056 pyroptosis for escape from macrophages. MBio *5*, e00003-14.
1057 72. Dufey, E., Bravo-San Pedro, J.M., Eggers, C., González-Quiroz, M., Urra, H., Sagredo, A.I.,
1058 Sepulveda, D., Pihán, P., Carreras-Sureda, A., Hazari, Y., et al. (2020). Genotoxic stress
1059 triggers the activation of IRE1α-dependent RNA decay to modulate the DNA damage
1060 response. Nat. Commun. *11*, 2401.
1061 73. Zhu, X., Zhang, J., Sun, H., Jiang, C., Dong, Y., Shan, Q., Su, S., Xie, Y., Xu, N., Lou, X., et
1062 al. (2014). Ubiquitination of inositol-requiring enzyme 1 (IRE1) by the E3 ligase CHIP
1063 mediates the IRE1/TRAF2/JNK pathway. J. Biol. Chem. *289*, 30567–30577.
1064 74. Urano, F., Wang, X., Bertolotti, A., Zhang, Y., Chung, P., Harding, H.P., and Ron, D. (2000).
1065 Coupling of stress in the ER to activation of JNK protein kinases by transmembrane protein
1066 kinase IRE1. Science *287*, 664–666.
1067 75. Ruland, J., and Hartjes, L. (2019). CARD-BCL-10-MALT1 signalling in protective and
1068 pathological immunity. Nat. Rev. Immunol. *19*, 118–134.
1069 76. Li, A., Song, N.-J., Riesenberg, B.P., and Li, Z. (2019). The Emerging Roles of Endoplasmic
1070 Reticulum Stress in Balancing Immunity and Tolerance in Health and Diseases: Mechanisms
1071 and Opportunities. Front. Immunol. *10*, 3154.
1072 77. Reimold, A.M., Iwakoshi, N.N., Manis, J., Vallabhajosyula, P., Szomolanyi-Tsuda, E.,
1073 Gravallese, E.M., Friend, D., Grusby, M.J., Alt, F., and Glimcher, L.H. (2001). Plasma cell
1074 differentiation requires the transcription factor XBP-1. Nature *412*, 300–307.
1075 78. Shaffer, A.L., Shapiro-Shelef, M., Iwakoshi, N.N., Lee, A.-H., Qian, S.-B., Zhao, H., Yu, X.,
1076 Yang, L., Tan, B.K., Rosenwald, A., et al. (2004). XBP1, downstream of Blimp-1, expands
1077 the secretory apparatus and other organelles, and increases protein synthesis in plasma cell
1078 differentiation. Immunity *21*, 81–93.
1079 79. Lee, A.-H., Heidtman, K., Hotamisligil, G.S., and Glimcher, L.H. (2011). Dual and opposing
1080 roles of the unfolded protein response regulated by IRE1alpha and XBP1 in proinsulin
1081 processing and insulin secretion. Proc. Natl. Acad. Sci. U. S. A. *108*, 8885–8890.
1082 80. Batista, A., Rodvold, J.J., Xian, S., Searles, S.C., Lew, A., Iwawaki, T., Almanza, G., Waller,
1083 T.C., Lin, J., Jepsen, K., et al. (2020). IRE1α regulates macrophage polarization, PD-L1
1084 expression, and tumor survival. PLoS Biol. *18*, e3000687.
1085 81. Pramanik, J., Chen, X., Kar, G., Henriksson, J., Gomes, T., Park, J.-E., Natarajan, K., Meyer,
1086 K.B., Miao, Z., McKenzie, A.N.J., et al. (2018). Genome-wide analyses reveal the IRE1a-
1087 XBP1 pathway promotes T helper cell differentiation by resolving secretory stress and
1088 accelerating proliferation. Genome Med. *10*, 76.
1089 82. Yadav, R.K., Chae, S.-W., Kim, H.-R., and Chae, H.J. (2014). Endoplasmic reticulum stress
1090 and cancer. J Cancer Prev *19*, 75–88.
1091 83. Sha, H., He, Y., Yang, L., and Qi, L. (2011). Stressed out about obesity: IRE1α-XBP1 in
1092 metabolic disorders. Trends Endocrinol. Metab. *22*, 374–381.
1093 84. Westman, J., Plumb, J., Licht, A., Yang, M., Allert, S., Naglik, J.R., Hube, B., Grinstein, S.,
1094 and Maxson, M.E. (2022). Calcium-dependent ESCRT recruitment and lysosome exocytosis
1095 maintain epithelial integrity during Candida albicans invasion. Cell Rep. *38*, 110187.

1096 85. Moretti, J., Roy, S., Bozec, D., Martinez, J., Chapman, J.R., Ueberheide, B., Lamming, D.W.,
1097 Chen, Z.J., Horng, T., Yeretssian, G., et al. (2017). STING Senses Microbial Viability to
1098 Orchestrate Stress-Mediated Autophagy of the Endoplasmic Reticulum. Cell *171*, 809-
1099 823.e13.
1100 86. Nunes-Hasler, P., and Demaurex, N. (2017). The ER phagosome connection in the era of
1101 membrane contact sites. Biochim. Biophys. Acta Mol. Cell Res. *1864*, 1513–1524.
1102 87. Thompson, H.L., and Wilton, J.M. (1992). Interaction and intracellular killing of Candida
1103 albicans blastospores by human polymorphonuclear leucocytes, monocytes and monocyte-
1104 derived macrophages in aerobic and anaerobic conditions. Clin. Exp. Immunol. *87*, 316–321.
1105 88. Blasi, E., Radzioch, D., Merletti, L., and Varesio, L. (1989). Generation of macrophage cell
1106 line from fresh bone marrow cells with a myc/raf recombinant retrovirus. Cancer Biochem.
1107 Biophys. *10*, 303–317.
1108 89. Hirota, M., Kitagaki, M., Itagaki, H., and Aiba, S. (2006). Quantitative measurement of spliced
1109 XBP1 mRNA as an indicator of endoplasmic reticulum stress. J. Toxicol. Sci. *31*, 149–156.
1110 90. Martin, M. (2011). Cutadapt removes adapter sequences from high-throughput sequencing
1111 reads. EMBnet J. *17*, 10.
1112 91. Bray, N.L., Pimentel, H., Melsted, P., and Pachter, L. (2016). Near-optimal probabilistic RNA-
1113 seq quantification. Nat. Biotechnol. *34*, 525–527.
1114 92. Love, M.I., Huber, W., and Anders, S. (2014). Moderated estimation of fold change and
1115 dispersion for RNA-seq data with DESeq2. Genome Biol. *15*, 550.
1116 93. Reimand, J., Kull, M., Peterson, H., Hansen, J., and Vilo, J. (2007). g:Profiler--a web-based
1117 toolset for functional profiling of gene lists from large-scale experiments. Nucleic Acids Res.
1118 *35*, W193-200.
1119 94. Ost, K.S., O'Meara, T.R., Stephens, W.Z., Chiaro, T., Zhou, H., Penman, J., Bell, R.,
1120 Catanzaro, J.R., Song, D., Singh, S., et al. (2021). Adaptive immunity induces mutualism
1121 between commensal eukaryotes. Nature *596*, 114–118.
1122 95. Stringer, C., Wang, T., Michaelos, M., and Pachitariu, M. (2021). Cellpose: a generalist
1123 algorithm for cellular segmentation. Nat. Methods *18*, 100–106.
1124 96. Allan, D.B., Caswell, T., Keim, N.C., van der Wel, C.M., and Verweij, R.W. (2024). soft-
1125 matter/trackpy: v0.6.2 (v0.6.2). Zenodo. 10.5281/zenodo.10696534.
1126 97. Virtanen, P., Gommers, R., Oliphant, T.E., Haberland, M., Reddy, T., Cournapeau, D.,
1127 Burovski, E., Peterson, P., Weckesser, W., Bright, J., et al. (2020). Author Correction: SciPy
1128 1.0: fundamental algorithms for scientific computing in Python. Nat. Methods *17*, 352.